Atmos. Chem. Phys. Discuss., 13, 19471–19525, 2013
www.atmos-chem-phys-discuss.net/13/19471/2013/
doi:10.5194/acpd-13-19471-2013

Atmospheric Chemistry and Physics Discussions

Global and regional emissions estimates for N_2O

E. Saikawa[1,2], R. G. Prinn[1], E. Dlugokencky[3], K. Ishijima[4], G. S. Dutton[3,5], B. D. Hall[3], R. Langenfelds[6], Y. Tohjima[7], T. Machida[7], M. Manizza[8], M. Rigby[9], S. O'Doherty[9], P. K. Patra[4], C. M. Harth[8], R. F. Weiss[8], P. B. Krummel[6], M. van der Schoot[6], P. B. Fraser[6], L. P. Steele[6], S. Aoki[10], T. Nakazawa[10], and J. W. Elkins[3]

[1]Center for Global Change Science, Massachusetts Institute of Technology, Cambridge, MA, USA
[2]Department of Environmental Studies, Emory University, Atlanta, GA, USA
[3]Earth System Research Laboratory, National Oceanic and Atmospheric Administration, Boulder, CO, USA
[4]Research Institute for Global Change, Japan Agency for Marine-Earth Science and Technology, Yokohama, Japan
[5]Cooperative Institute for Research in Environmental Sciences, University of Colorado, Boulder, CO 80309, USA
[6]Centre for Australian Weather and Climate Research, CSIRO Marine and Atmospheric Research, Aspendale, Victoria, Australia
[7]National Institute for Environmental Studies, Tsukuba, Japan
[8]Scripps Institution of Oceanography, University of California, San Diego, La Jolla, California, USA

[9]School of Chemistry, University of Bristol, Bristol, UK
[10]Center for Atmospheric and Oceanic Studies, Tohoku University, Sendai, Japan

Received: 19 June 2013 – Accepted: 25 June 2013 – Published: 23 July 2013

Correspondence to: E. Saikawa (eri.saikawa@emory.edu)

Published by Copernicus Publications on behalf of the European Geosciences Union.

Abstract

We present a comprehensive estimate of nitrous oxide (N_2O) emissions using observations and models from 1995 to 2008. High-frequency records of tropospheric N_2O are available from measurements at Cape Grim, Tasmania; Cape Matatula, American Samoa; Ragged Point, Barbados; Mace Head, Ireland; and at Trinidad Head, California using the Advanced Global Atmospheric Gases Experiment (AGAGE) instrumentation and calibrations. The Global Monitoring Division of the National Oceanic and Atmospheric Administration/Earth System Research Laboratory (NOAA/ESRL) has also discrete air samples collected in flasks and in situ measurements from remote sites across the globe and analyzed them for a suite of species including N_2O. In addition to these major networks, we include in situ and aircraft measurements from the National Institute for Environmental Studies (NIES) and flask measurements from the Tohoku University and Commonwealth Scientific and Industrial Research Organization (CSIRO) networks. All measurements show increasing atmospheric mole fractions of N_2O, with a varying growth rate of 0.1–0.7 % yr^{-1}, resulting in a 7.4 % increase in the background atmospheric mole fraction between 1979 and 2011. Using existing emission inventories as well as bottom-up process modeling results, we first create globally-gridded a priori N_2O emissions over the 37 yr since 1975. We then use the three-dimensional chemical transport model, Model for Ozone and Related Chemical Tracers version 4 (MOZART v4), and a Bayesian inverse method to estimate global as well as regional annual emissions for five source sectors from 13 regions in the world. This is the first time that all of these measurements from multiple networks have been combined to determine emissions. Our inversion indicates that global and regional N_2O emissions have an increasing trend between 1995 and 2008. Despite large uncertainties, a significant increase is seen from the Asian agricultural sector in the recent years, most likely due to an increase in the use of nitrogenous fertilizers, as has been suggested by previous studies, and also in Asian natural soil.

ACPD
13, 19471–19525, 2013

1 Introduction

Nitrous oxide (N_2O) is a potent greenhouse gas (GHG) with a global warming potential (GWP) approximately 300 times greater than CO_2 over a 100 yr time horizon (Forster et al., 2007). N_2O is also involved in stratospheric ozone depletion (Crutzen, 1970), and although its ozone-depletion potential (ODP) is as small as 0.017, its emissions, weighted by ODP, currently is larger than those of any other ozone-depleting substances (ODSs) (Ravishankara et al., 2009). Importantly, N_2O emissions are controlled under the Kyoto Protocol, but N_2O production is not included in the Montreal Protocol on substances that deplete the Ozone Layer. N_2O is inert in the troposphere and is only destroyed once it reaches the stratosphere by photolysis and by chemical reaction with $O(^1D)$. Because of the inertness within the troposphere, N_2O has a long atmospheric lifetime of 131 ± 10 yr (Prather et al., 2012).

There are several known sources of N_2O emissions, and in this paper we categorize them as the following: agricultural soil, industrial (including all combustion sources), natural soil, ocean, and biomass burning. There are large uncertainties associated with estimated emissions from each of these sectors, but approximately 2/3 of the emissions has been attributed to natural sources (natural soil and ocean), and the remaining from anthropogenic (Khalil et al., 2002; Denman et al., 2007; Nevison et al., 2007). Included in our industrial source category are major emissions from land use change, fuel combustion for energy, and waste (European Commission, Joint Research Centre (JRC)/Netherlands Environmental Assessment Agency (PBL), 2009). The increase in atmospheric N_2O mixing ratios since at least 1940 has been largely attributed to increased N_2O emissions from agricultural soils (Park et al., 2012).

Previous work has examined the source and the magnitude of these emissions with process models ("bottom-up") and with inverse methods using measurements of atmospheric mixing ratios ("top-down"). For the former, there have been efforts to quantify soil and ocean emissions. For example, Potter et al. (1996) estimated global soil N_2O emissions using an ecosystem modeling approach. Using the "hole-in-the-

ACPD
13, 19471–19525, 2013

pipe" concept established by Firestone and Davidson (1989) and simulating with an expanded version of the Carnegie–Ames–Stanford (CASA) Biosphere model (Potter et al., 1993), they estimated the global N_2O emissions from soil to be 6.1 Tg N_2O–N yr^{-1}. For global soil N_2O emissions excluding anthropogenic nitrogen input effects, Bouwman et al. (1993) and Kreileman and Bouwman (1994) estimated emissions to be 6.6–7.0 Tg N_2O–N yr^{-1}. Using the DeNitrification–DeComposition (DNDC) model developed by Li et al. (1992), Saikawa et al. (2013) estimated global natural soil N_2O emissions from 1975 to 2008 with four different available forcing datasets. Annual average estimates range from 7.4–11 Tg N_2O–N yr^{-1}. For the ocean emissions, Nevison et al. (1995) used more than 60 000 expedition measurements to estimate global annual outgassing from the ocean to be 1.2–6.8 Tg N_2O–N yr^{-1}. Recently, Manizza et al. (2012) used a large-scale ocean general circulation model coupled to a biogeochemical model to quantify the climatological mean emissions from the ocean to be 4.5 Tg N_2O–N yr^{-1}.

For the top-down approach, previous work has derived global and regional N_2O emissions using the existing emissions inventories and atmospheric N_2O measurements. Prinn et al. (1990) conducted inverse modeling of N_2O at the global level using a 12-box model and quantified emissions from four latitudinal bands in the world. Hirsch et al. (2006) used a three-dimensional chemical transport model to estimate N_2O emissions from global, four semihemispherical and six broad regions between 1998 and 2001. Their results showed that there may have been a shift in emissions from 30°–90° S to 0°–30° N during the period 1978–1988 to 1998–2001. Huang et al. (2008) estimated N_2O emissions during the two time periods (1997–2001 and 2002–2005), using a three-dimensional chemical transport model and estimated the global N_2O emissions to be 15.1–17.8 and 14.1–17.1 Tg N_2O–N yr^{-1} in the two periods, respectively. Kort et al. (2011) found that inversion results differ between including and excluding aircraft measurements and emphasized the importance of measurements covering the full tropospheric profile.

ACPD
13, 19471–19525, 2013

In this paper, drawing on insights from recent "bottom-up" estimates using four different forcing datasets for global natural soil emissions (Saikawa et al., 2013) and the climatological ocean emissions (Manizza et al., 2012), we first estimate approximate "bottom-up" monthly regional sectoral N_2O emissions on a global grid during 1995–2008. We use these gridded emissions as an a priori estimate for an inversion to derive regional and global emission magnitudes from the atmospheric observations. For this work, we present the new observations until the end of 2008 and use them as well as previously published N_2O atmospheric mole fraction data from several measurement networks as listed in Fig. 1 and Table 1. The goal of the paper was to include, for the first time, all available measurements (i.e., in situ, flasks, aircrafts, and ships) from several networks where we have reliable and consistent inter-comparison of measurements.

The paper is organized as follows: Section 2 describes the atmospheric measurements. Section 3 explains the inverse modeling methodology. Section 4 examines results from our inversion to analyze regional sectoral emissions. We present a summary of our results and suggestions for future research in Sect. 5.

2 Archived and ambient measurements

In this study, we use measurements of atmospheric N_2O from six networks: (1) in situ measurements from the Advanced Global Atmospheric Gases Experiment (AGAGE) network; (2) the Global Monitoring Division of NOAA's Earth System Research Laboratory (NOAA/ESRL) Carbon Cycle Greenhouse Gases (CCGG) group global cooperative air sampling flask network; (3) the NOAA/ESRL Halocarbons and other Atmospheric Trace Species (HATS) discrete sample (flask) (OTTO) and in situ (Radiatively Important Trace Species, RITS and Chromatograph for Atmospheric Trace Species, CATS) network; (4) the Commonwealth Scientific and Industrial Research Organization (CSIRO) flask sampling network; (5) the National Institute for Environmental Studies (NIES) in situ and Surgut aircraft measurement network, and (6) the Tohoku University

ACPD
13, 19471–19525, 2013

flask measurement network. We use them for our inversions to estimate emissions of N_2O. Within the AGAGE network, high-frequency in situ measurements of N_2O have been carried out using gas chromatography with electron capture detection (GC/ECD) (Prinn et al., 2000) at five sites since 1978. In this study, we use measurements of air sampled at the following AGAGE sites: Cape Grim, Tasmania; Trinidad Head, California, USA; Mace Head, Ireland; Ragged Point, Barbados; Cape Matatula, American Samoa (see Fig. 1 and Table 1). Stations that previously existed at Cape Meares, Oregon (1979–1989) and at Adrigole, Ireland (1978–1983) were replaced by Trinidad Head and Mace Head, respectively. All AGAGE in situ measurements are calibrated using the SIO-98 absolute calibration scale. The estimate of all the errors involved in the calibration scale such as reagent purity, possible analytical interferences, statistics of primary standard preparation, and propagation is approximately 0.5 %.

At NOAA/ESRL, discrete air samples have been collected at remote locations and analyzed for N_2O since 1997 as part of the Carbon Cycle Greenhouse Gases (CCGG) global cooperative air sampling network (Dlugokencky et al., 1994). Samples of air are collected regularly in paired glass flasks (2–3 L) and pressurized to 0.20 MPa, and analyzed on one of two GC/ECD instruments in Boulder, Colorado. In this study, we use measurements from 72 sites (Fig. 1 and Table 1). Repeatability of the analytical system is 0.2 ppb (1σ), and the total uncertainty including reagent purity, interferences, etc. is 1.0 ppb (0.3 %).

In situ and flask measurements are also collected by the NOAA HATS program over the globe. The NOAA RITS in situ program started at the following four stations in 1987: Barrow, AK, USA; Mauna Loa, HI, USA; Cape Matatula, American Samoa; and South Pole, as well as in Niwot Ridge, CO, USA in 1990. The CATS program started using new in situ gas chromatographs at all of the above-mentioned five sites, and also added Summit, Greenland in 2007. The OTTO program has also collected flasks at weekly to monthly intervals from the above six stations as well as seven other following sites: Alert, Canada; Cape Kumukahi, HI, USA; Cape Grim, Australia; Palmer Station, Antarctica; Mace Head, Ireland; Trinidad Head, CA, USA; Tierra del Fuego, Argentina.

ACPD
13, 19471–19525, 2013

All NOAA measurements are on the NOAA-2006A N_2O scale (Hall et al., 2007), and the estimate of all the errors for the RITS, CATS, and OTTO programs is less than 0.4 ppb (0.1 %) (Hall et al., 2007).

We also use flask measurements from the CSIRO network (Francey et al., 1996, 2003). There are eleven measurement sites including the one at Cape Rama, India (Fig. 1 and Table 1). The flasks have been collected at weekly to monthly intervals at these sites and are analyzed by GC/ECD at CSIRO. The measurements are referenced to the NOAA-2006A N_2O scale (Hall et al., 2007). Repeatability of the analytical system is 0.3 ppb (1σ), and the estimate of the error in accuracy is less than 0.1 % for the majority of the samples.

NIES has been measuring N_2O at two field sites (Hateruma Island and Cape Ochi-ishi, see Fig. 1 and Table 1). These N_2O measurements are calibrated using the NIES-96 scale (Tohjima et al., 2000). The precision of the measurement system is approximately 0.3 ppb (1σ) and the estimate of the error in accuracy is approximately 0.4 ppb (0.1 %).

Monthly aircraft measurements have been made near the city of Surgut, Russia since July 1993, using a chartered aircraft as described in Ishijima et al. (2010). Outside air is collected at 0.5, 1, 1.5, 2, 3, 4, 5.5, and 7 km above the surface in glass flasks, pressurized and then analyzed by an GC/ECD instrument in NIES. The NIES-96 N_2O scale is used for calibration, and the repeatability of the analytical system is 0.3 ppb. The estimate of the error in accuracy is approximately 0.4 ppb (0.1 %).

The Tohoku University group has been measuring N_2O at multiple locations using aircraft and ships since 1991 (Ishijima et al., 2001, 2009, 2010). Collected air samples are analyzed using the GC/ECD at the Tohoku University. The data between 2003 and 2009 are new and cover a wide range surrounding Japan (see Fig. 1). These N_2O measurements are calibrated using the Tohoku University scale. Repeatability of the flask samples is 1.0 ppb until 2001 and 0.3 ppb since 2002, and the estimate of the error in accuracy is approximately 0.2 %.

ACPD
13, 19471–19525, 2013

We compare measurements collected from each group as they are based on different absolute calibration scales (Table 2) and differences exist among measurement networks. Because the global average mole fraction of N_2O increases at approximately 0.2–0.3 % per year (see Fig. 2), the calibration ratio of 0.9975 corresponds to a one year's rise in mole fraction, and thus the calibration difference of as small as 0.6 % can be significant. Hence, it is very important for us to adjust all of the measurements into a single scale, even though calibration appears to be fairly close to each other. First, the comparisons between AGAGE and NOAA are conducted using measurements collected at the same site at approximately the same time. NOAA CCGG flask samples collected at the four AGAGE sites (CGO, SMO, RPB, and MHD) between 1997 and 2012 and at THD between 2002 and 2012 were compared with AGAGE GC-ECD in situ measurements at those sites. Data from the two networks agree well in general for N_2O with a mean ratio (CCGG/AGAGE) of 0.9994 and a standard deviation of 0.0005 for the matching mixing ratios. In addition, NOAA CATS in situ samples collected at SMO from 2000 to 2012 were compared with AGAGE GC-ECD in situ measurements at the same site. The data also agree well with a mean ratio (CATS/AGAGE) of 1.0009 and a standard deviation of 0.0010. RITS measurements compare well with CATS, and thus we use the same factor for both. We therefore adjust the NOAA measurements to the SIO-98 scale by applying 1.0006 for CCGG flask and 0.9991 for OTTO, RITS, and CATS in our inversions. We also apply an offset factor for the measurements taken in the OTTO network as a difference from the CATS measurements at the same site. The adjustment is 1.3 ppb at American Samoa and 0.6 ppb elsewhere.

Second, the comparisons between the AGAGE and CSIRO networks are conducted at the CGO site, where the average difference is 0.35 ppb (AGAGE – CSIRO), which is equivalent to the ratio (CSIRO/AGAGE) of 0.9989. Therefore, we adjust the CSIRO flask network measurements by applying a factor of 1.0011 in our inversions.

Third, the comparisons between NOAA CATS and Tohoku University as well as between NIES and Tohoku University are conducted at the same site at approximately the same time. On average, Tohoku University measurements are 0.2 ppb and 0.8 ppb

ACPD
13, 19471–19525, 2013

higher than NOAA and NIES measurements, respectively. These values translate into the mean ratios (Tohoku/CATS and Tohoku/NIES) of about 1.0006 and 1.0025. These two comparisons also allow us to quantify the constant off-set values between CATS and NIES measurements (CATS – NIES) of 0.6 ppb with a ratio (CATS/NIES) of approximately 1.0019. Based on these comparisons, the ratios (Tohoku/AGAGE and NIES/AGAGE) are approximately 1.0015 and 0.9990. Therefore, we apply 0.9985 and 1.0011 to convert Tohoku and NIES measurements into the SIO-98 scale.

3 Emissions inversion method

Using reasonable prior estimates of annual sectoral and regional N_2O emissions and the three-dimensional chemical transport model, Model for Ozone and Related Chemical Tracers version 4 (MOZART v4), we apply an inverse method to estimate annual sectoral and regional emissions using the measurements of N_2O atmospheric mole fractions discussed above. In this section, we outline our inverse modeling methodology.

3.1 Prior emission estimate

For conducting inversions, we created a priori emission estimates by combining the existing emissions inventory for the three sectors (i.e., industrial, agricultural soil, and biomass burning) with new estimates from two process models for ocean and natural soil. For industrial and agricultural soil emissions, we used the EDGAR v4.1 emissions with a spatial resolution of 1° latitude × 1° longitude (European Commission, Joint Research Centre (JRC)/Netherlands Environmental Assessment Agency (PBL), 2009). EDGAR provides gridded emissions every 5 yr between 1970 and 2000, and annually between 2000 and 2005. We therefore interpolated annual emissions based on the growth rate to fill gaps and extrapolated to 2008 by taking the average annual growth rate between 2001 and 2005. For biomass burning emissions, we used the Global Fire

ACPD
13, 19471–19525, 2013

Emissions Database version 3 (GFED v3) with a spatial resolution of 0.5° latitude × 0.5° longitude (van der Werf et al., 2010). GFED v3 provides monthly emissions between 1997 and 2008, so we extrapolated for years between 1990 and 1996 by applying the average annual growth rate between 1997 and 2008.

Manizza et al. (2012) estimated climatological monthly air-sea N_2O fluxes using a "bottom-up" process modeling approach. Their model includes both denitrification and nitrification process-induced fluxes at a spatial resolution of 2.8° latitude × 2.8° longitude. They adopted the parameterization of Suntharalingam and Sarmiento (2000) for the production of N_2O in the water column. A more detailed description of their physical and biogeochemical model can be found in Manizza et al. (2012).

For natural soil emissions, we use another newly developed process model (CLMCN-N_2O) that reproduces the seasonality and inter-annual variability of global emissions (Saikawa et al., 2013). This model is an addition to the Community Land Model with coupled Carbon and Nitrogen cycles version 3.5 (CLM-CN v3.5) (Thornton et al., 2007, 2009; Randerson et al., 2009). CLMCN-N_2O includes the DeNitrification–DeComposition (DNDC) Biogeochemistry Model (Li et al., 1992), and similarly to the ocean process model, it captures both the nitrification and denitrification processes that are important producers of N_2O in soil. Four forcing datasets used are: Global Meteorological Forcing Dataset (GMFD); NCEP Corrected by CRU (NCC); Climate Analysis Section (CAS); and Global Offline Land–Surface Dataset (GOLD), and a more detailed description of the model and the forcing datasets can be found in Saikawa et al. (2013).

For our regional inversion, we assume 40 % uncertainty for our prior values for the emissions from all sources, sectors, and regions. This range, decided empirically based on previous studies, is justifiable as there have been high uncertainties in N_2O emissions, especially in recent years after increased agricultural nitrogen fertilizer use in developing countries.

ACPD
13, 19471–19525, 2013

3.2 Global chemical transport model

The global three-dimensional chemical transport model, MOZART v4 (Emmons et al., 2010) is used to simulate the three-dimensional N_2O atmospheric mole fractions between 1995 and 2008. MOZART v4 is a model for the troposphere, has updates over the previous MOZART version 2, and is built on the framework of the Model of Atmospheric Transport and Chemistry (MATCH) (Rasch et al., 1997). Previous studies have found too strong net downward transport from the stratosphere in the model using the reanalysis meteorology (Holloway et al., 2000; van Noije et al., 2004; Xiao et al., 2010) resulting, for example, in errors in the tropospheric ozone budget as well as in the ozone mixing ratios in the upper troposphere (Emmons et al., 2010). Because this can lead to a potentially large bias in our analysis, we restricted ourselves to estimating regional and sectoral annual and not monthly emissions. This however provides new annual estimates for 14 yr at the regional and the sectoral level globally, which is an advancement from past studies. The horizontal resolution of MOZART v4 is 1.9° latitude × 2.5° longitude, including 56 vertical levels from the surface to approximately 2 hPa. Chemical and transport processes are driven by the annually-varying Modern Era Retrospective-analysis for Research and Applications (MERRA) meteorological fields (Rienecker et al., 2011).

We assume that N_2O is inert in the troposphere and chemical loss is by photolysis and reaction with $O(^1D)$ in the stratosphere. The spatial and temporal pattern of the inter-annually changing photolysis field is calculated for three wavelength-ranges 200–217 nm, 217–230 nm and 230–278 nm, and it includes the temperature dependency of the absorption cross sections, similarly to Ishijima et al. (2010). For the wavelength band 178–200 nm, Minschwaner et al. (1993) is used. The annually-repeating $O(^1D)$ field is estimated using the LMDZ4-INCA2 global climate model (Hourdin et al., 2006). Both of these fields are interpolated to match our horizontal and vertical resolutions, conserving the mass. The lifetime of N_2O, calculated by the ratio of the annual total global burden to the loss rate calculated in the chemical transport model is 116 ± 5 yr,

ACPD
13, 19471–19525, 2013

which is slightly lower than the current estimates of its lifetime (Prather et al., 2012) but is in alignment with Montzka et al. (2011).

We estimate emissions from 7 land regions and 6 ocean regions for 5 source sectors between 1995 and 2008 incorporating all the measurements in Table 1, including all data without pollution event filtering. The MERRA meteorological reanalyses were used at 6 hourly intervals, and the model was run with a 15 min time step. When there were measurements from multiple different networks, we first generated monthly averages for each network at each site, and then combined the datasets to create monthly averages and standard deviations at a site using the number of measurement-weighted averages, taking the measurement density of networks into account.

3.3 Sensitivity estimates and inverse method

To conduct inverse modeling, we need an estimate of how atmospheric mole fractions at each measurement site respond to an increase in emissions for each sector and region (which we herein call the "sensitivity"). For this purpose, we first ran the global chemical transport model MOZART v4 with the prior emissions discussed in Sect. 3.1 to yield a reference run. Next, we perturbed sectoral regional emissions by increasing them by 100 % for each sector, region, and year, one at a time while leaving the emissions for the other sectors, regions, and years unperturbed and ran MOZART v4. (c.f. Chen and Prinn, 2006).

We then tracked atmospheric mole fractions in the perturbed runs for two years (first year when the emissions are increased and the second year after the emissions return to the same level as the prior emissions) and compared them to the reference mole fractions. Because N_2O regional emissions are approximately mixed globally in two years, the response of the increased atmospheric mole fractions after this period is similar at all sites. Therefore, we assume that the perturbed mole fractions exponentially decrease to the globally well-mixed values after the end of the second year at all measurement sites, regardless of the regions and sectors (Chen and Prinn, 2006; Rigby et al., 2010; Saikawa et al., 2012). We calculate the sensitivity to a change in

ACPD
13, 19471–19525, 2013

emissions by dividing the increase in mole fraction by the increase in emissions from the regional sectoral total at each measurement site and incorporate these values into a sensitivity matrix **H** as used in the equation below.

We estimate emissions by deriving a Bayesian weighted least-squares solution using these calculated sensitivities (Prinn, 2000; Rigby et al., 2010; Saikawa et al., 2012). This technique provides an optimal estimate by minimizing the following cost function with respect to $\boldsymbol{x}$:

$$\boldsymbol{J} = (\boldsymbol{y} - \mathbf{H}\boldsymbol{x})^T \mathbf{W}^{-1} (\boldsymbol{y} - \mathbf{H}\boldsymbol{x}) + \boldsymbol{x}^T \mathbf{S}^{-1} \boldsymbol{x} \quad (1)$$

where $\boldsymbol{y}$ is the vector of the difference between measurements and modeled mole fractions, **H** is the sensitivity matrix, $\boldsymbol{x}$ is the vector of the difference between the prior and the optimized emissions, **W** is the measurement uncertainty covariance matrix, and **S** is the prior uncertainty covariance matrix. **W** and **S** are both diagonal matrices.

By combining the information from both measurements and prior emissions and weighting these by their respective inverse squared uncertainties, we obtain an optimal estimate of sectoral regional emissions for each year, sector, and region of interest. We show that sectoral and regional emissions can be constrained well, with a substantial reduction in posterior emissions uncertainty, by using the measurements from different network stations between 1995 and 2008. In some regions and especially in the ocean in some years we see little uncertainty reduction due to the lack of data.

3.4 Measurement-model uncertainty estimation

For total measurement uncertainty (whose squares (variances) are contained in the measurement covariance matrix **W**), four types of uncertainty were considered: errors in the measurements themselves (precision), scale propagation error, sampling frequency error, and model-data mismatch error. The total variance is therefore calculated by combining the four types as follows, assuming that they are uncorrelated (e.g.,

ACPD
13, 19471–19525, 2013

Chen and Prinn, 2006; Rigby et al., 2010; Saikawa et al., 2012):

$$\sigma^2 = \sigma^2_{\text{measurement}} + \sigma^2_{\text{scale propagation}} + \sigma^2_{\text{sampling frequency}} + \sigma^2_{\text{mismatch}} \quad (2)$$

Here the measurement error $\sigma_{\text{measurement}}$ is the estimated total uncertainty due to the repeatability of each measurement (precision) at each site. The instrumental precision of N_2O is approximately 0.1 % for AGAGE, NOAA CCGG, NIES, and CSIRO, 0.2 % for NOAA OTTO, RITS, and CATS, and 0.3 % before 2002 and 0.1 % since 2002 for Tohoku University, and thus these values are included as our instrumental precision errors for in this study.

The error $\sigma_{\text{scale propagation}}$ arises in the chain that links the primary standards to ambient air measurements. For N_2O, the mean assumed scale propagation error was approximately 0.006–0.012 % for all the SIO, 0.07 % for NOAA CCGG and OTTO, RITS, and CATS, 0.016 % for CSIRO, and 0.015–0.03 % for NIES and Tohoku University scales, respectively. We therefore include 0.012 %, 0.07 %, 0.016 %, and 0.03 % for all the data that come from AGAGE, for NOAA, for CSIRO, and for NIES and Tohoku University, respectively.

The error $\sigma_{\text{sampling frequency}}$ accounts for the number of samples measured in a month to create a monthly mean for each measurement site (Chen and Prinn, 2006). For example, the high-frequency in situ measurements provide a more accurate estimate of the monthly averaged mole fraction compared to a few flask measurements taken in a month. We quantify this uncertainty as the standard error of the monthly measurement, assuming temporally uncorrelated data (Chen and Prinn, 2006). Because of the difference in the number of measurements in a month between high-frequency observations (every 2 h) and weekly flask measurements, this error is approximately three to ten times lower for high-frequency observations, compared with the error associated with NOAA and AGAGE measurements at the same site. Even when we assume a 10 h serial correlation for the AGAGE in situ measurements (resulting in approximately 70 uncorrelated measurements in a month), it does not affect the results in any substantial way (the largest difference being less than 0.5 % change in optimized emissions).

ACPD
13, 19471–19525, 2013

The error σ_{mismatch} describes the difference between a point measurement and a model-simulated observation that represents a large volume of air (Prinn, 2000; Chen and Prinn, 2006). By assuming that the difference in modeled atmospheric mole fractions between the grid cell containing the measurement site and the eight cells surrounding the measurement site provides a reasonable estimate of this uncertainty, we calculate it from the following equation:

$$\sigma_{\text{mismatch}} = \sqrt{\frac{1}{8}\sum_{i=1}^{8}(y_i - y)^2} \quad (3)$$

where y_i is the atmospheric mole fraction in a grid box surrounding the measurement site location i, and y is the mole fraction in the grid cell at the measurement site. Similarly to the sampling frequency error, the mismatch error also varies by month at each site, taking into account the monthly changes in transport in the model.

4 Sectoral and regional emissions between 1995–2008

In this section, we present results from our regional inversion to derive sectoral regional N_2O emissions for the 13 regions using all available data from AGAGE, NOAA CCGG, NOAA OTTO, RITS, and CATS, CSIRO, NIES, and Tohoku University networks (Fig. 1 and Table 1), as well as MOZART v4. We seek to determine the locations and magnitudes of these emissions, and if we see any change in the recent years from a specific region or sector.

We created the regions based on their proximity to the measurement sites, and with the intention of separating emissions based on large ocean groups. For those areas very distant from these sites the regions are entire continents, and if there are sufficient measurements, we divided the continent into multiple regions. The closer a given region is to a measurement site, the larger sensitivity to emission perturbations in that region we would expect.

ACPD
13, 19471–19525, 2013

The seven land regions in this study are: (1) Africa and Middle East; (2) Central and South America; (3) Northern Asia; (4) Southern Asia; (5) Europe; (6) North America; and (7) Oceania (see Fig. 3). Asia is divided into two, because there are multiple measurement stations in the region. This division within Asia is also of interest, because there is high uncertainty in the winter soil emissions in the higher latitude regions such as in Russia, covered under "Northern Asia". China under "Southern Asia" is by far the largest consumer of nitrogen fertilizer between 1995 and 2008, as shown in Fig. 4 (International Fertilizer Industry Association). Its total nitrogen consumption is more than twice larger than that of India, the second largest consumer since 2004 before the United States, also under "Southern Asia". The six ocean regions in this study are: (1) North Pacific; (2) South Pacific; (3) Northern Ocean; (4) Atlantic; (5) Southern Ocean; and (6) Indian Ocean (see Fig. 3).

We conduct regional inversions using four sets of a priori emissions for 1995 through 2008. The four sets differ only in natural soil emissions due to the different estimates that come from the four different forcing datasets used in the bottom-up estimates for this sector, and there is no difference in other sectors. We conduct an inversion using all measurements available including AGAGE, NOAA, CSIRO, NIES, and Tohoku University networks. We find that by emission sector, the largest uncertainty reduction is for natural soil and, by region, it is for Northern Asia. We achieve these results because natural soil has the largest emissions among all sources and because we have the largest number of long-standing stations close to our Northern Asia region, as can be seen in Fig. 1. Figure 3 provides the prior and posterior emissions with uncertainty bars for all the sectors and regions quantified from this inversion, and Table 3 provides prior and posterior emissions with uncertainties for global total, global land, and sectoral total emissions. Table 4 lists prior and optimized emissions with uncertainties for each region, and Tables 5–8 provide prior and optimized emissions derived from this inversion for each sector and region using all the measurements.

ACPD
13, 19471–19525, 2013

4.1 Sectoral emissions trend

We find an increasing trend in agricultural soil emissions in many regions, but Southern Asia – the region that includes China and India – shows the most significant signal (see Fig. 3a and Table 5). Inter-annual variability is visible in the result, but emissions in recent years are still statistically significantly larger than the estimates for 1995 and 1996, and this aligns well with a recent study showing increased N_2O emissions due to agriculture (Park et al., 2012). The five-year mean agricultural soil emissions between 2004–2008 (3.8 $Tg\,N_2O–N\,yr^{-1}$) is 28 % greater than the mean from 1995–1999 (3.0 $Tg\,N_2O–N\,yr^{-1}$).

Natural soil emissions also show significant inter-annual variability especially in Northern and Southern Asia (see Fig. 3c and Table 7). Furthermore, the five-year mean natural soil emissions between 2004–2008 (2.5 $Tg\,N_2O–N\,yr^{-1}$) is 33 % greater than that from 1995–1999 (1.9 $Tg\,N_2O–N\,yr^{-1}$) for Southern Asia. On the other hand, there is no significant increase in Northern Asia for natural soil emissions. We also realize that there are anti-correlations contained and derived in state-vector error covariance matrix (**W**) in some of the estimates we find due to the nature of our inversion methodology. Between Southern Asia agricultural and natural soil emissions, the average correlation value is −0.36, showing a high anti-correlation. This illustrates that we are unable to differentiate the two source emissions (natural vs. agricultural), but given that both are showing increase, we are confident of the increasing N_2O emissions from soil in Southern Asia.

We further find a high anti-correlation (−0.76) between Northern and Southern Asia for natural soil especially for 2006, when Northern Asia natural soil emissions estimates are very low. The average correlation value between all regions was −0.0055, and the average value between these two regions for natural soil was −0.36, excluding 2006. Interestingly, however, compared to the differences in the prior emissions estimates from the four different forcing datasets, the optimized emissions converge relatively well, giving us confidence in the inversion results. Our optimized ocean emissions are

ACPD
13, 19471–19525, 2013

also within the range of the climatological prior in most years. At the same time, we also see some impact of El Niño Southern Oscillation (ENSO) events on natural soil and ocean emissions. Some of these inter-annual variabilities we find in natural emissions are qualitatively correlated with ENSO events, but the effect of ENSO on sources and sinks of these emissions are complex (Davidson et al., 2004) and it is beyond the scope of this paper. More discussions can be found in Saikawa et al. (2013) for natural soil emissions.

We do not find much inter-annual variability in other sector emissions including industrial and biomass burning. The main reason is because those emissions are smaller compared to the natural soil and ocean emissions, which lead to sensitivities also being equally small. Therefore, we do not obtain a large uncertainty reduction from our inversion as seen in Figs. 3b and 3e. The only exception where we find a decreased emissions trend is in Southern Asia biomass burning, where emissions in recent years are much smaller than during the 1990s. However, this is simply due to the prior emissions estimates and is not due to our inversion, as can be seen by the small uncertainty reduction.

4.2 Regional emissions trend

For North America, our mean optimized emissions between 2004 and 2008 are $1.18 \pm 0.22\,\mathrm{Tg\,N_2O{-}N\,yr^{-1}}$ (Table 4). Here and in all subsequent discussions, the uncertainties we list are one standard deviation. Miller et al. (2012) analyzed tall tower observations in 2004 and 2008 using a Lagrangian model and found peak emissions in June over the central United States. Jeong et al. (2012) have looked at emissions from central California from December 2007 through November 2009, using measurements from a tall tower (Walnut Grove), and they also found posterior emissions to be twice the EDGAR emission inventory estimates. Similarly, Kort et al. (2008), using measurements from the CO_2 Budget and Regional Airborne–North America (COBRA-NA) campaign in May–June 2003 and a Lagrangian model, estimated annual N_2O emissions from North America to be 2.7 $\mathrm{Tg\,N_2O{-}N\,yr^{-1}}$. As Miller et al. (2012) indicates,

ACPD
13, 19471–19525, 2013

extrapolating these results to the US and Canada results in this region accounting for 12–15 % of the total N_2O source and 32–39 % of the global anthropogenic source in 2007. Our estimate suggests that North America is 5.9–8.0 % of the total N_2O source and 21.1–26.9 % of the global anthropogenic source, and they differ from these previous estimates. The discrepancies may be due to these regional inversion results being based on a short-term data and from selected sites whereas our study uses data from six measurement networks with extensive spatial coverage to constrain the global budget. Short-term and regional inversion results might not be appropriate to constrain annual N_2O emissions. At the same time, there is a significant difference in the Lagrangian and Eulerian models that are worth investigating.

Our estimates however agree quite well with other Lagrangian-based studies done in Europe. For example, Corazza et al. (2011) used NOAA/ESRL measurements and a four-dimensional variational (4DVAR) technique with an atmospheric transport zoom model to estimate European emissions in 2006 and quantified annual European N_2O emissions to be 0.76 $Tg\,N_2O–N\,yr^{-1}$, and this value is in alignment with ours ($0.85 \pm 0.10\,Tg\,N_2O–N\,yr^{-1}$). Manning et al. (2003) derived annual EU N_2O emissions between 1995 and 2000 using the Numerical Atmospheric Dispersion Modeling Environment (NAME) model driven by three-dimensional synoptic meteorology from the Unified Model. Their estimated range, 0.84–0.88 $Tg\,N_2O–N\,yr^{-1}$, also agrees with our estimate of $0.81 \pm 0.23\,Tg\,N_2O–N\,yr^{-1}$ for the same period. Our result is also in alignment with Thompson et al. (2011) who used observations from a tower site at Ochsenkopf, Germany and a Lagrangian model to estimate western and central European emissions at a weekly time step in 2007, and found emissions peaked during August and September.

For Asia, Yan et al. (2003), using a bottom-up approach, estimated agricultural emissions from Asian countries (including China, India, Pakistan, Indonesia, Thailand, Philippines, Bangladesh, Myanmar, Viet Nam, Japan, and others) for 1995 to be 1.19 $Tg\,N_2O–N\,yr^{-1}$. Our result for agricultural soil from the same region in 1995 is

ACPD
13, 19471–19525, 2013

$0.82 \pm 0.12\,Tg\,N_2O–N\,yr^{-1}$, which is slightly smaller, but this may be due to the difference in the countries included in our estimates.

For North America, Europe, and Oceania, we also compared our posterior estimates using GMFD forcing dataset for natural soil with Intergovernmental Panel on Climate Change (IPCC) Fourth Assessment Report (AR4) estimates (Denman et al., 2007) (Fig. 5). For North America and Europe, our estimates are lower than the IPCC estimates for anthropogenic N_2O emissions. For both North America and Europe, our posterior estimates in 2008 are closer to the IPCC estimates than in 1995 due to our increased agricultural soil estimates from the region, but there is a large discrepancy in Europe due to a much larger estimate in agricultural soil in their estimate. For Oceania, our estimates are higher than IPCC, mainly due to our prior estimates being higher than their estimates. As mentioned earlier, there is little uncertainty reduction in Oceania due to little sensitivities from measurements in this region (Fig. 3).

We also compared global land and global ocean emissions with the previous estimates. Comparing the global total land budget from our inversions with other previous estimates, we find good agreement. Hirsch et al. (2006) estimated the global total land emissions to be $15.2–20.4\,Tg\,N_2O–N\,yr^{-1}$ for the period between 1998 and 2001. Our estimate of $17.1 \pm 0.71\,Tg\,N_2O–N\,yr^{-1}$ is in their range. The global ocean emissions estimates vary from as low as $0.90–1.7\,Tg\,N_2O–N\,yr^{-1}$ (Rhee et al., 2009), $1.2–6.8\,Tg\,N_2O–N\,yr^{-1}$ (Nevison et al., 1995), $3.8\,Tg\,N_2O–N\,yr^{-1}$ (Suntharalingam and Sarmiento, 2000), $4.5\,Tg\,N_2O–N\,yr^{-1}$ (Manizza et al., 2012), $4.5–6.5\,Tg\,N_2O–N\,yr^{-1}$ (Hirsch et al., 2006), to as high as $5.8–7.8Tg\,N_2O–N\,yr^{-1}$ (Nevison et al., 2003). Our estimates agree with the median value and the average among the 14 yr of our calculation is $4.88 \pm 0.43\,Tg\,N_2O–N\,yr^{-1}$.

The global total that we find from this study is consistent with results from past studies. Our results for the two time periods (1997–2001 and 2002–2005) are 17.02 ± 0.74 and $18.0 \pm 0.69\,Tg\,N_2O–N\,yr^{-1}$, respectively, and they are not significantly different from the ranges estimated by Huang et al. (2008) for the same period (15.1–17.8 and 14.1–$17.1\,Tg\,N_2O–N\,yr^{-1}$, respectively). Our results for 1998–2001 ($17.1 \pm 0.71\,Tg\,N_2O–$

ACPD
13, 19471–19525, 2013

$N\,yr^{-1}$) also compare well with those by Hirsch et al. (2006) (15.2–20.4 $Tg\,N_2O$–$N\,yr^{-1}$). Furthermore, our global total emissions estimate results in ODP-weighted emissions of 0.48 Mt CFC-11-e, and this is larger than the sum of the ODS emissions of those controlled by the Montreal Protocol (approximately 0.45 Mt CFC-11-e) (Daniel et al., 2011).

Our results also indicate that the ratio of anthropogenic (including agricultural soil, industrial, and biomass burning) to natural (natural soil and ocean) emissions has increased in recent years in Southern Asia and in Central/South America. In addition to Southern Asia, Central and South America is where we have seen a 49 % increase in nitrogen fertilizer consumption between 1995 and 2008 (International Fertilizer Industry Association). Indeed, the 5 yr mean of anthropogenic emissions show shifts from 69.3 % between 1995–1999 to 79.0 % between 2004–2008 in Southern Asia, and similarly from 44.0 % to 47.9 % in Central/South America. These results indicate, however, that the natural emissions still share approximately 2/3 of the global total N_2O emissions, as has been discussed in the past.

4.3 Inversions using different measurements

In addition to using all measurements, we conducted separate inversions as follows: (1) only including the in situ measurements (AGAGE, NIES, and NOAA RITS, CATS); (2) only including the flask measurements (Surgut aircraft, NOAA CCGG, and OTTO, Tohoku University, and CSIRO); and (3) only including AGAGE and NOAA CCGG measurements. We chose these three options because of several reasons. First, by selecting only the in situ and the flask measurements, these comparisons allow us to determine the importance of spatial and temporal resolutions of the measurements in estimating regional and sectoral emissions. Second, we excluded measurements that had significant calibration difference to understand how calibration differences could impact the inversion results. For example, AGAGE and NOAA CCGG are on very similar standard scales as shown by frequent comparisons of all measurements, whereas

ACPD
13, 19471–19525, 2013

all others have gone through some minor adjustment. Figure 6 shows the uncertainty reduction for natural soil emissions in seven regions for each inversion.

We find that in all regions except for North America, inversions using all measurements provide the largest uncertainty reduction for natural soil emission estimates most of the time (see Fig. 6). In North America, we achieve the largest uncertainty reductions when including only flask data. The reason why the largest uncertainty reduction is not achieved when using all available measurements in this region is due to the differences in measured values at several sites. There are several such as BRW, MHD, and NWR, where more than three different measurement networks are co-located, and although we do apply ratios to minimize these differences (as explained in Sect. 2), Fig. 6 illustrates that these scale differences still limit our ability to constrain regional emissions. This highlights the need for unification of standard scales and more ongoing measurement comparisons among networks.

In all cases, only including in situ measurements results in the smallest uncertainty reduction due to the spatial sparsity of the data after 1997, when a significant number of NOAA CCGG measurements start. Figure 6 also illustrates that consistency and wide coverage of the measurements are both very important, especially for analyzing sectoral and regional emissions. However, it is important to point out the differences between in situ and flask measurements. In situ measurements are high-frequency measurements that are able to collect a random subset of total N_2O data at a particular site, whereas flask data are for representing the background air at a site. In our coarse-resolution modeling, it is often not possible to make the best use of high-frequency in situ measurements. Such difference between the two measurement networks are especially visible in Europe and Oceania, where the regional coverage is small.

There are several ways we could improve the accuracy of N_2O emissions inferred from inverse modeling in the future. First, expanding measurements in data-sparse regions such as Africa, Middle East, Eastern Europe, South Asia, Central/South America, Oceania, Atlantic Ocean, Indian Ocean, northern and Southern Oceans would allow us to better constrain emissions from these regions, which in turn would also improve

ACPD
13, 19471–19525, 2013

the global emission estimate. Second, the use of finer-resolution chemical transport models and meteorology data would also allow us to disaggregate regions further and detect sensitivities to atmospheric mole fractions due to increases in emissions more accurately. In the future, we could potentially combine a global Eulerian model with a Lagrangian model to focus on a specific region of interest (Rigby et al., 2011). Third, conducting inversions using various chemical transport models rather than a single one as we did here will enable us to better quantify the uncertainty related to model bias and transport error, as has been done for carbon dioxide (Baker et al., 2006). Fourth, including the whole stratosphere (e.g., using the Whole Atmosphere Community Climate Model) may improve stratosphere-troposphere interactions, possibly leading to a improved simulation of monthly variability that we observe in the measurements.

5 Conclusions

We utilized published and new atmospheric mole fraction measurements of N_2O between 1995–2008 from six measurement networks (AGAGE, NOAA CCGG, NOAA OTTO, RITS, and CATS, CSIRO, NIES, and Tohoku University), comprised of archived air samples, flask measurements at daily, weekly, and monthly frequency (surface, towers, aircrafts, and ships), and high-frequency in situ observations to derive regional and sectoral emission estimates. This is the first time that such an almost all-inclusive comprehensive dataset has been utilized for an inverse study of N_2O. We estimated regional (seven land and six ocean) and sectoral (agricultural soil, industrial, natural soil, ocean, and biomass burning) emissions of N_2O from 1995–2008 using these measurements and the global three-dimensional chemical transport model MOZART v4 with a Bayesian inverse methodology. Our estimated emissions generally agree with previously published estimates, although there are major discrepancies in North America between our results and those of Miller et al. (2012); Jeong et al. (2012) and Kort et al. (2008) using a Lagrangian model.

ACPD
13, 19471–19525, 2013

Our regional inversion results indicate no significant emissions increase or reduction in all sectors except agricultural soil, and we find inter-annual variability in soil and ocean emissions. Global total emissions have been increasing in recent years, and we find a significant increasing trend in agricultural soil emissions from Southern Asia, which includes China and India, mostly due to the rise in nitrogen fertilizers in these developing economies, as suggested in the past studies (Davidson, 2009; Park et al., 2012). In addition, we find that the anthropogenic emissions are increasing in Southern Asia and in Central/South America, most likely due to the increase in these agricultural soil emissions.

We do not necessarily obtain the largest uncertainty reduction for our optimized emissions by utilizing all available data. Our inversion results using different combinations of measurements illustrate the importance of unifying measurement scales, as well as broad spatial coverage for regional and sectoral emissions estimates. More research is essential to accurately assess regional emissions at a finer scale, especially to investigate the impact of different models used in the study, but we show that soil is the largest source of N_2O emissions and that our optimized N_2O emissions estimate results in ODP-weighted emissions larger than the sum of the ODS emissions of those controlled by the Montreal Protocol.

Acknowledgements. The AGAGE research program is supported by the NASA Upper Atmospheric Research Program in the US with grants NNX11AF17G to MIT, NNX07AF09G and NNX07AE87G to SIO, Defra/DECC contract GA0201 for support of the Mace Head measurements and NOAA contract RA133R09CN0062 for partial support of Ragged Point in Barbados, CSIRO and the Australian Government Bureau of Meteorology in Australia. For this study MM acknowledges financial support from the post-doctoral fellowship at Scripps Institution of Oceanography and from NASA, grant NNX08AB48G. NOAA provided operational support of the AGAGE systems at American Samoa. NOAA HATS support comes from the NOAA Climate Program Office under their Atmospheric Chemistry, Carbon Cycle, and Climate (AC4) Program. We would like to thank Arlyn Andrews, Nada Derek, Rona Thompson, David Nance, and Debra Mondeel for their help. We also thank all the staff at the AGAGE, NOAA, CSIRO, NIES, and To-

ACPD
13, 19471–19525, 2013

hoku University sites for their contributions to produce high quality measurements of important atmospheric trace gases.

References

Baker, D. F., Law, R. M., Gurney, K. R., Rayner, P., Peylin, P., Denning, A. S., Bousquet, P., Bruhwiler, L., Chen, Y. H., Ciais, P., Fung, I. Y., Heimann, M., John, J., Maki, T., Maksyutov, S., Masarie, K., Prather, M., Pak, B., Taguchi, S., and Zhu, Z.: TransCom 3 inversion intercomparison: impact of transport model errors on the interannual variability of regional CO_2 fluxes, 1988–2003, Global Biogeochem. Cy., 20, GB1002, doi:10.1029/2004GB002439, 2006. 19494

Bouwman, A. F., Fung, I., Matthews, E., and John, J.: Global analysis of the potential for N_2O production in natural soils, Global Biogeochem. Cy., 7, 557–597, doi:10.1029/93GB01186, 1993. 19475

Chen, Y.-H., and Prinn, R. G.: Estimation of atmospheric methane emissions between 1996 and 2001 using a three-dimensional global chemical transport model, J. Geophys. Res., 111, doi:10.1029/2005JD006058, 2006. 19483, 19485, 19486

Corazza, M., Bergamaschi, P., Vermeulen, A. T., Aalto, T., Haszpra, L., Meinhardt, F., O'Doherty, S., Thompson, R., Moncrieff, J., Popa, E., Steinbacher, M., Jordan, A., Dlugokencky, E., Brühl, C., Krol, M., and Dentener, F.: Inverse modelling of European N_2O emissions: assimilating observations from different networks, Atmos. Chem. Phys., 11, 2381–2398, doi:10.5194/acp-11-2381-2011, 2011. 19490

Crutzen, P. J.: The influence of nitrogen oxides on the atmospheric ozone content, Q. J. Roy. Meteor. Soc., 96, 320–325, doi:10.1002/qj.49709640815, 1970. 19474

Daniel, J. S., Velders, G. J. M., Morgenstern, O., Toohey, D. W., Wallington, T. J., Wuebbles, D. J., Akiyoshi, H., Bais, A. F., Fleming, E. L., Jackman, C. H., Kuijpers, L. J. M., McFarland, M., Montzka, S. A., Ross, M. N., Tilmes, S., Tully, M. B., Andersen, S. O., Langematz, U., and Mingley, P. M.: A Focus on Information on Options for Policymakers, chap. 5, 52, Global Ozone Research and Monitoring Project Report, 2011. 19492

Davidson, E. A.: The contribution of manure and fertilizer nitrogen to atmospheric nitrous oxide since 1860, Nat. Geosci., 2, 659–662, doi:10.1038/ngeo608, 2009. 19495

ACPD
13, 19471–19525, 2013

Davidson, E. A., Ishida, F. Y., and Nepstad, D. C.: Effects of an experimental drought on soil emissions of carbon dioxide, methane, nitrous oxide, and nitric oxide in a moist tropical forest, Glob. Change Biol., 10, 718–730, doi:10.1111/j.1529-8817.200300762.x, 2004. 19489

Denman, K. L., Brasseur, G., Chidthaisong, A., Ciais, P., Cox, P. M., Dickinson, R. E., Hauglustaine, D., Heinze, C., Holland, E., Jacob, D., Lohmann, U., Ramachandran, S., Leite da Silva Dias, P., Wofsy, S. C., and Zhang, X.: Couplings between changes in the climate system and biogeochemistry, chap. 7, Cambridge University Press, Cambridge, United Kingdom and New York, NY, USA, 2007. 19474, 19491

Dlugokencky, E. J., Steele, L. P., Lang, P. M., and Masarie, K. A.: The growth rate and distribution of atmospheric methane, J. Geophys. Res., 99, 17021–17043, doi:10.1029/94JD01245, 1994. 19477

Emmons, L. K., Walters, S., Hess, P. G., Lamarque, J.-F., Pfister, G. G., Fillmore, D., Granier, C., Guenther, A., Kinnison, D., Laepple, T., Orlando, J., Tie, X., Tyndall, G., Wiedinmyer, C., Baughcum, S. L., and Kloster, S.: Description and evaluation of the Model for Ozone and Related chemical Tracers, version 4 (MOZART-4), Geosci. Model Dev., 3, 43–67, doi:10.5194/gmd-3-43-2010, 2010. 19482

European Commission, Joint Research Centre (JRC)/Netherlands Environmental Assessment Agency (PBL): Emission Database for Global Atmos. Res.(EDGAR), release version 4.0, available at: http://edgar.jrc.ec.europa.eu, last access: 2 July 2013. 2009. 19474, 19480

Firestone, M. K. and Davidson, E. A.: Microbiological basis of NO and N2O production and consumption in soil, John Wiley and Sons, New York, NY, 7–21, 1989. 19475

Forster, P., Ramaswamy, V., Artaxo, P., Berntsen, T., Betts, R., Fahey, D. W., Haywood, J., Lean, J., Lowe, D. C., Myhre, G., Nganga, J., Prinn, R., Raga, G., Schulz, M., and van Dorland, R.: Changes in Atmospheric Constituents and in Radiative Forcing, chap. 2, Cambridge University Press, United Kingdom and New York, NY, 129–234, 2007. 19474

Francey, R. J., Steele, L. P., Langenfelds, R. L., Lucarelli, M. P., Allison, C. E., Beardsmore, D. J., Coram, S. A., Derek, N., de Silva, F. R., Etheridge, D. M., Fraser, P. J., Henry, R. J., Turner, B., Welch, E. D., Spencer, D. A., and Cooper, L. N.: Global Atmospheric Sampling Laboratory (GASLAB): supporting and extending the Cape Grim trace gas programs, Bureau of Meteorology and CSIRO Division of Atmospheric Research, 8–29, 1996. 19478

Francey, R. J., Steele, L. P., Spencer, D. A., Langenfelds, R. L., Law, R. M., Krummel, P. B., Fraser, P. J., Etheridge, D. M., Derek, N., Coram, S. A., Cooper, L. N., Allison, C. E., Porter, L., and Baly, S.: The CSIRO (Australia) measurement of greenhouse gases in the global atmo-

ACPD
13, 19471–19525, 2013

sphere, World Meteorological Organization Global Atmosphere Watch, report of the 11th WMO/IAEA Meeting of Experts on Carbon Dioxide Concentration and Related Tracer Measurement Techniques, Tokyo, Japan, September 2001, edited by: Toru, S. and Kazuto, S., 8–29, 2003. 19478

Hall, B. D., Dutton, G. S., and Elkins, J. W.: The NOAA nitrous oxide standard scale for atmospheric observations, J. Geophys. Res., 112, D09305, doi:10.1029/2006JD007954, 2007. 19478

Hirsch, A. I., Michalak, A. M., Bruhwiler, L. M., Peters, W., Dlugokencky, E. J., and Tans, P. P.: Inverse modeling estimates of the global nitrous oxide surface flux from 1998–2001, Global Biogeochem. Cy., 20, GB1008, doi:10.1029/2004GB002443, 2006. 19475, 19491, 19492

Holloway, T., Levy, Hiram, I., and Kasibhatla, P.: Global distribution of carbon monoxide, J. Geophys. Res., 105, 12123–12147, doi:10.1029/1999JD901173, 2000. 19482

Hourdin, F., Musat, I., Bony, S., Braconnot, P., Codron, F., Dufresne, J.-L., Fairhead, L., Filiberti, M.-A., Friedlingstein, P., Grandpeix, J.-Y., Krinner, G., LeVan, P., Li, Z.-X., and Lott, F.: The LMDZ4 general circulation model: climate performance and sensitivity to parametrized physics with emphasis on tropical convection, Clim. Dynam., 27, 787–813, doi:10.1007/s00382-006-0158-0, 2006. 19482

Huang, J., Golombek, A., Prinn, R., Weiss, R., Fraser, P., Simmonds, P., Dlugokencky, E. J., Hall, B., Elkins, J., Steele, P., Langenfelds, R., Krummel, P., Dutton, G., and Porter, L.: Estimation of regional emissions of nitrous oxide from 1997 to 2005 using multinetwork measurements, a chemical transport model, and an inverse method, J. Geophys. Res., 113, D17313, doi:10.1029/2007JD009381, 2008. 19475, 19491

International Fertilizer Industry Association: IFA, http://www.fertilizer.org/ifa/ifadata, last access: 26 May 2013, 2013. 19487, 19492, 19521

Ishijima, K., Nakazawa, T., Sugawara, S., Aoki, S., and Saeki, T.: Concentration variations of tropospheric nitrous oxide over Japan, Geophys. Res. Lett., 28, 171–174, doi:10.1029/2000GL011465, 2001. 19478

Ishijima, K., Nakazawa, T., and Aoki, S.: Variations of atmospheric nitrous oxide concentration in the northern and western Pacific, Tellus B, 61, 408–415, doi:10.1111/j.1600-0889.2008.00406.x, 2009. 19478

Ishijima, K., Patra, P. K., Takigawa, M., Machida, T., Matsueda, H., Sawa, Y., Steele, L. P., Krummel, P. B., Langenfelds, R. L., Aoki, S., and Nakazawa, T.: Stratospheric influence on the seasonal cycle of nitrous oxide in the troposphere as deduced from aircraft observations

ACPD
13, 19471–19525, 2013

and model simulations, J. Geophys. Res., 115, D20308, doi:10.1029/2009JD013322, 2010. 19478, 19482

Jeong, S., Zhao, C., Andrews, A. E., Dlugokencky, E. J., Sweeney, C., Bianco, L., Wilczak, J. M., and Fischer, M. L.: Seasonal variations in N_2O emissions from central California, Geophys. Res. Lett., 39, L16805, doi:10.1029/2012GL052307, 2012. 19489, 19494

Khalil, M. A. K., Rasmussen, R. A., and Shearer, M. J.: Atmospheric nitrous oxide: patterns of global change during recent decades and centuries, Chemosphere, 47, 807–821, doi:10.1016/S0045-6535(01)00297-1, 2002. 19474

Kort, E. A., Eluszkiewicz, J., Stephens, B. B., Miller, J. B., Gerbig, C., Nehrkorn, T., Daube, B. C., Kaplan, J. O., Houweling, S., and Wofsy, S. C.: Emissions of CH_4 and N_2O over the United States and Canada based on a receptor-oriented modeling framework and COBRA-NA atmospheric observations, Geophys. Res. Lett., 35, L18808, doi:10.1029/2008GL034031, 2008. 19489, 19494

Kort, E. A., Patra, P. K., Ishijima, K., Daube, B. C., Jimenez, R., Elkins, J., Hurst, D., Moore, F. L., Sweeney, C., and Wofsy, S. C.: Tropopsheric distribution and variability of N_2O: evidence for strong tropical emissions, Geophys. Res. Lett., 38, L15806, doi:10.1029/2011GL047612, 2011. 19475

Kreileman, G. J. J. and Bouwman, A. F.: Computing land use emissions of greenhouse gases, Water, Air, and Soil Pollution, 76, 231–258, doi:10.1007/BF00478341, 1994. 19475

Li, C., Frolking, S., and Frolking, T. A.: A model of nitrous oxide evolution from soil driven by rainfall events: 1. Model structure and sensitivity, J. Geophys. Res., 97, 9759–9776, 1992. 19481

Manizza, M., Keeling, R. F., and Nevison, C. D.: On the processes controlling the seasonal cycles of the air-sea fluxes of O_2 and N_2O: A modelling study, Tellus B, 64, 18429, doi:10.3402/tellusb.v64i0.18429, 2012. 19475, 19476, 19481, 19491

Manning, A. J., Ryall, D. B., Derwent, R. G., Simmonds, P. G., and O'Doherty, S.: Estimating European emissions of ozone-depleting and greenhouse gases using observations and a modeling back-attribution technique, J. Geophys. Res.-Atmos., 108, 4405, doi:10.1029/2002JD002312, 2003. 19490

Miller, S. M., Kort, E. A., Hirsch, A. I., Dlugokencky, E. J., Andrews, A. E., Xu, X., Tian, H., Nehrkorn, T., Eluszkiewicz, J., Michalak, A. M., and Wofsy, S. C.: Regional sources of nitrous oxide over the United States: seasonal variation and spatial distribution, J. Geophys. Res., 117, D06310, doi:10.1029/2011JD016951, 2012. 19489, 19494

ACPD
13, 19471–19525, 2013

Minschwaner, K., Salawitch, R. J., and McElroy, M. B.: Absorption of solar radiation by O_2: implications for O_3 and lifetimes of N_2O, $CFCl_3$, and CF_2Cl_2, J. Geophys. Res.-Atmos., 98, 10543–10561, doi:10.1029/93JD00223, 1993. 19482

Montzka, S. A., Authors), S. R. C. L., Engel, A., Krüger, K., O'Doherty, S., Sturges, W. T., Blake, D., Dorf, M., Fraser, P., Froidevaux, L., Jucks, K., Kreher, K., Kurylo, M. J., Mellouki, A., Miller, J., Nielsen, O.-J., Orkin, V. L., Prinn, R. G., Rhew, R., Santee, M. L., Stohl, A., and Verdonik, D.: Ozone-Depleting Substances (ODSs) and Related Chemicals, chap. 1, p. 516, 52, Global Ozone Research and Monitoring Project - Report, Geneva, Switzerland, 2011. 19483

Nevison, C., Butler, J. H., and Elkins, J. W.: Global distribution of N_2O and the ΔN_2O-AOU yield in the subsurface ocean, Global Biogeochem. Cy., 17, 1119, doi:10.1029/2003GB002068, 2003. 19491

Nevison, C. D., Weiss, R. F., and Erickson, D. J.: Global oceanic emissions of nitrous oxide, J. Geophys. Res., 100, 15809–15820, 1995. 19475, 19491

Nevison, C. D., Mahowald, N. M., Weiss, R. F., and Prinn, R. G.: Interannual and seasonal variability in atmospheric N_2O, Global Biogeochem. Cy., 21, GB3017, doi:10.1029/2006GB002755, 2007. 19474

Park, S., Croteau, P., Boering, K. A., Etheridge, D. M., Ferretti, D., Fraser, P. J., Kim, K.-R., Krummel, P. B., Langenfelds, R. L., van Ommen, T. D., Steele, L. P., and Trudinger, C. M.: Trends and seasonal cycles in the isotopic composition of nitrous oxide since 1940, Nat. Geosci., 5, 261–265, doi:10.1038/ngeo1421, 2012. 19474, 19488, 19495

Potter, C. S., Randerson, J. T., Field, C. B., Matson, P. A., Vitousek, P. M., Mooney, H. A., and Klooster, S. A.: Terrestrial ecosystem production: A process model based on global satellite and surface data, Global Biogeochem. Cy., 7, 811–841, doi:10.1029/93GB02725, 1993. 19475

Potter, C. S., Matson, P. A., Vitousek, P. M., and Davidson, E. A.: Process modeling of controls on nitrogen trace gas emissions from soils worldwide, J. Geophys. Res., 101, 1361–1377, 1996. 19474

Prather, M. J., Holmes, C. D., and Hsu, J.: Reactive greenhouse gas scenarios: systematic exploration of uncertainties and the role of atmospheric chemistry, Geophys. Res. Lett., 39, L09803, doi:10.1029/2012GL051440, 2012. 19474, 19483

Prinn, R. G.: Measurement equation for trace chemicals in fluids and solution of its inverse, in: Inverse Methods in: Global Biogeochemical Cycles, edited by: Kashibhatla, P., Heimann, M.,

ACPD
13, 19471–19525, 2013

Rayner, P., Mahowald, N., Prinn, R. G., and Hartley, D. E., vol. 114 of Geophys. Monogr. Ser., 3–18, AGU, 2000. 19484, 19486

Prinn, R. G., Cunnold, D., Rasmussen, R., Simmonds, P., Alyea, F., Crawford, A., Fraser, P., and Rosen, R.: Atmospheric emissions and trends of nitrous oxide deduced from 10 years of ALE-GAGE data, J. Geophys. Res., 95, 18369–18385, 1990. 19475

Prinn, R. G., Weiss, R. F., Fraser, P. J., Simmonds, P. G., Cunnold, D. M., Alyea, F. N., O'Doherty, S., Salameh, P., Miller, B. R., Huang, J., Wang, R. H. J., Hartley, D. E., Harth, C., Steele, L. P., Sturrock, G., Midgley, P. M., and McCulloch, A.: A history of chemically and radiatively important gases in air deduced from ALE/GAGE/AGAGE, J. Geophys. Res., 105, 17751–17792, doi:10.1029/2000JD900141, 2000. 19477

Randerson, J. T., Hoffman, F. M., Thornton, P. E., Mahowald, N. M., Lindsay, K., Lee, Y. H., Nevison, C. D., Doney, S. C., Bonan, G., Stockli, R., Covey, C., Running, S. W., and Fung, I. Y.: Systematic Assessment of Terrestrial Biogeochemistry in Coupled Climate-Carbon Models, Glob. Change Biol., 15, 2462–2484, 2009. 19481

Rasch, P. J., Mahowald, N. M., and Eaton, B. E.: Representations of transport, convection, and the hydrologic cycle in chemical transport models: implications for the modeling of short-lived and soluble species, J. Geophys. Res., 102, 28127–28138, doi:10.1029/97JD02087, 1997. 19482

Ravishankara, A. R., Daniel, J. S., and Portmann, R. W.: Nitrous oxide (N_2O): the dominant ozone-depleting substance emitted in the 21st century, Science, 326, 123–125, available at: http://www.jstor.org/stable/40328592, 2009. 19474

Rhee, T. S., Kettle, A. J., and Andreae, M. O.: Methane and nitrous oxide emissions from the ocean: a reassessment using basin-wide observations in the Atlantic, J. Geophys. Res.-Atmos., 114, E12304, doi:10.1029/2008JD011662, 2009. 19491

Rienecker, M. M., Suarez, M. J., Gelaro, R., Todling, R., Bacmeister, J., Liu, E., Bosilovich, M. G., Schubert, S. D., Takacs, L., Kim, G.-K., Bloom, S., Chen, J., Collins, D., Conaty, A., da Silva, A., Gu, W., Joiner, J., Koster, R. D., Lucchesi, R., Molod, A., Owens, T., Pawson, S., Pegion, P., Redder, C. R., Reichle, R., Robertson, F. R., Ruddick, A. G., Sienkiewicz, M., and Woollen, J.: MERRA: NASA's Modern-Era Retrospective Analysis for Research and Applications, J. Climate, 24, 3624–3648, doi:10.1175/JCLI-D-11-00015.1, 2011. 19482

Rigby, M., Mühle, J., Miller, B. R., Prinn, R. G., Krummel, P. B., Steele, L. P., Fraser, P. J., Salameh, P. K., Harth, C. M., Weiss, R. F., Greally, B. R., O'Doherty, S., Simmonds, P. G.,

ACPD
13, 19471–19525, 2013

Vollmer, M. K., Reimann, S., Kim, J., Kim, K.-R., Wang, H. J., Olivier, J. G. J., Dlugokencky, E. J., Dutton, G. S., Hall, B. D., and Elkins, J. W.: History of atmospheric SF_6 from 1973 to 2008, Atmos. Chem. Phys., 10, 10305–10320, doi:10.5194/acp-10-10305-2010, 2010. 19483, 19484, 19485

Rigby, M., Manning, A. J., and Prinn, R. G.: Inversion of long-lived trace gas emissions using combined Eulerian and Lagrangian chemical transport models, Atmos. Chem. Phys., 11, 9887–9898, doi:10.5194/acp-11-9887-2011, 2011. 19494

Saikawa, E., Rigby, M., Prinn, R. G., Montzka, S. A., Miller, B. R., Kuijpers, L. J. M., Fraser, P. J. B., Vollmer, M. K., Saito, T., Yokouchi, Y., Harth, C. M., Mühle, J., Weiss, R. F., Salameh, P. K., Kim, J., Li, S., Park, S., Kim, K.-R., Young, D., O'Doherty, S., Simmonds, P. G., McCulloch, A., Krummel, P. B., Steele, L. P., Lunder, C., Hermansen, O., Maione, M., Arduini, J., Yao, B., Zhou, L. X., Wang, H. J., Elkins, J. W., and Hall, B.: Global and regional emission estimates for HCFC-22, Atmos. Chem. Phys., 12, 10033–10050, doi:10.5194/acp-12-10033-2012, 2012. 19483, 19484, 19485

Saikawa, E., Schlosser, C. A., and Prinn, R.: Global modeling of soil nitrous oxide emissions from natural processes, Global Biogeochem. Cy., in review, 2013. 19475, 19476, 19481, 19489

Suntharalingam, P. and Sarmiento, J. L.: Factors governing the oceanic nitrous oxide distribution: simulations with an ocean general circulation model, Global Biogeochem. Cy., 14, 429–454, doi:10.1029/1999GB900032, 2000. 19481, 19491

Thompson, R. L., Gerbig, C., and Rödenbeck, C.: A Bayesian inversion estimate of N_2O emissions for western and central Europe and the assessment of aggregation errors, Atmos. Chem. Phys., 11, 3443–3458, doi:10.5194/acp-11-3443-2011, 2011. 19490

Thornton, P. E., Lamarque, J. F., Rosenbloom, N. A., and Mahowald, N. M.: Influence of carbon-nitrogen cycle coupling on land model response to CO_2 fertilization and climate variability, Global Biogeochem. Cy., 21, GB4018, doi:10.1029/2006GB002868, 2007. 19481

Thornton, P. E., Doney, S. C., Lindsay, K., Moore, J. K., Mahowald, N., Randerson, J. T., Fung, I., Lamarque, J.-F., Feddema, J. J., and Lee, Y.-H.: Carbon-nitrogen interactions regulate climate-carbon cycle feedbacks: results from an atmosphere-ocean general circulation model, Biogeosciences, 6, 2099–2120, doi:10.5194/bg-6-2099-2009, 2009. 19481

Tohjima, Y., Mukai, H., Maksyutov, S., Takahashi, Y., Machida, T., Katsumoto, M., and Fujinuma, Y.: Variations in atmospheric nitrous oxide observed at Hateruma monitoring station, Chemosphere, 2, 435–443, 2000. 19478

ACPD
13, 19471–19525, 2013

van der Werf, G. R., Randerson, J. T., Giglio, L., Collatz, G. J., Mu, M., Kasibhatla, P. S., Morton, D. C., DeFries, R. S., Jin, Y., and van Leeuwen, T. T.: Global fire emissions and the contribution of deforestation, savanna, forest, agricultural, and peat fires (1997–2009), Atmos. Chem. Phys., 10, 11707–11735, doi:10.5194/acp-10-11707-2010, 2010. 19481

van Noije, T. P. C., Eskes, H. J., van Weele, M., and van Velthoven, P. F. J.: Implications of the enhanced Brewer-Dobson circulation in European Centre for Medium-Range Weather Forecasts reanalysis ERA-40 for the stratosphere-troposphere exchange of ozone in global chemistry transport models, J. Geophys. Res., 109, D19308, doi:10.1029/2004JD004586, 2004. 19482

Xiao, X., Prinn, R. G., Fraser, P. J., Weiss, R. F., Simmonds, P. G., O'Doherty, S., Miller, B. R., Salameh, P. K., Harth, C. M., Krummel, P. B., Golombek, A., Porter, L. W., Butler, J. H., Elkins, J. W., Dutton, G. S., Hall, B. D., Steele, L. P., Wang, R. H. J., and Cunnold, D. M.: Atmospheric three-dimensional inverse modeling of regional industrial emissions and global oceanic uptake of carbon tetrachloride, Atmos. Chem. Phys., 10, 10421–10434, doi:10.5194/acp-10-10421-2010, 2010. 19482

Yan, X., Akimoto, H., and Ohara, T.: Estimation of nitrous oxide, nitric oxide and ammonia emissions from croplands in East, Southeast and South Asia, Glob. Change Biol., 9, 1080–1096, doi:10.1046/j.1365-2486.2003.00649.x, 2003. 19490

ACPD
13, 19471–19525, 2013

Table 1a. N_2O measurement site information.

Station	Code	Lat. (° N)	Long. (° E)	Alt. (m a.s.l.)	Data Period Used[1]	Network	Type
South Pole	SPO	−90	−24.8	2810	Jan 1995–Dec 2008	CSIRO	flask
					Jan 1995–Dec 2008	NOAA CCGG&OTTO	flask
					Jan 1995–Dec 2008	NOAA RITS&CATS	in situ
Halley Station, Antarctica	HBA	−75.6	−26.21	35.0	Feb 1996–Dec 2008	NOAA CCGG	flask
Syowa Station, Antarctica	SYO	−69.0	39.58	11.0	Feb 1997–Dec 2008	NOAA CCGG	flask
Mawson, Antarctica	MAA	−67.62	62.87	32.0	Jan 1995–Dec 2008	CSIRO	flask
Casey, Antarctica	CYA	−66.28	110.52	60.0	Nov 1996–Dec 2008	CSIRO	flask
Palmer Station, Antarctica	PSA	−64.92	−64.00		Apr 1997–Dec 2008	NOAA CCGG & OTTO	flask
Drake Passage	DRP	−59	−64.69	10	Apr 2003–Dec 2008	NOAA CCGG	flask
Tierra Del Fuego, Argentina	TDF	−54.85	−68.31	32	Jun 1997–Dec 2008	NOAA CCGG & OTTO	flask
Macquarie Island, Australia	MQA	−54.48	158.97	12	Jan 1995–Dec 2008	CSIRO	flask
Crozet Island, France	CRZ	−46.43	51.85	202	Nov 1996–Dec 2008	NOAA CCGG	flask
Baring Head Station, New Zealand	BHD	−41.42	174.87	95.0	Oct 1999–Dec 2008	NOAA CCGG	flask
Cape Grim, Tasmania	CGO	−40.68	144.69	21	Jan 1995–Dec 2008	CSIRO	flask
					Jan 1995–Dec 2008	AGAGE	in situ
					Jan 1996–Dec 2008	NOAA CCGG&OTTO	flask
Easter Island, Chile	EIC	−27.15	−109.45	55.0	Jul 1997–Dec 2008	NOAA CCGG	flask
Gobabeb, Namibia	NMB	−23.58	15.03	461	Aug 1997–Dec 2008	NOAA CCGG	flask
Cape Ferguson, Australia	CFA	−19.28	147.06	2.0	Jan 1995–Dec 2008	CSIRO	flask
Cape Matatula, Samoa	SMO	−14.23	−170.56	77	Mar 1996–Dec 2008	AGAGE	in situ
					Jan 1995–Dec 2008	NOAA CCGG&OTTO	flask
					Jan 1995–Dec 2008	NOAA RITS&CATS	in situ
Arembepe, Brazil	ABP	−12.76	−38.16	6.0	Oct 2006–Dec 2008	NOAA CCGG	flask
Ascension Island, UK	ASC	−7.97	−14.4	90	Aug 1997–Dec 2008	NOAA CCGG	flask
Mahe Island, Seychelles	SEY	−4.68	55.53	3.0	Jun 1997–Dec 2008	NOAA CCGG	flask
Bukit Kototabang, Indonesia	BKT	−0.2	100.32	850.0	Jan 2004–Dec 2008	NOAA CCGG	flask
Mt. Kenya, Kenya	MKN	−0.06	37.3	3649	Dec 2003–Dec 2008	NOAA CCGG	flask
Christmas Island, Republic of Kiribati	CHR	1.70	−157.15	2.0	Sep 1997–Dec 2008	NOAA CCGG	flask
Ragged Point, Barbados	RPB	13.17	−59.43	45	Jun 1996–Dec 2008	AGAGE	in situ
					Nov 1995–Dec 2008	NOAA CCGG	flask
Mariana Islands, Guam	GMI	13.39	144.66	6.0	Dec 1995–Dec 2008	NOAA CCGG	flask
Cape Rama, India	CRI	15.08	73.83	66	Jan 1995–Dec 2008	CSIRO	flask
Cape Kumakahi, HI, USA	KUM	19.52	−154.82	3	Jan 1995–Dec 2008	NOAA CCGG&OTTO	flask
Mauna Loa, HI, USA	MLO	19.50	−155.60	3397	Jan 1995–Dec 2008	CSIRO	flask
					Jan 1995–Dec 2008	NOAA CCGG&OTTO	flask
					Jan 1995–Dec 2008	NOAA RITS&CATS	in situ
Assekrem, Algeria	ASK	23.18	5.42	1847	Dec 1996–Dec 2008	NOAA CCGG	flask
Lulin, Taiwan	LLN	23.46	120.86	2867	Aug 2006–Dec 2008	NOAA CCGG	flask
Hateruma, Japan	HAT	24.05	123.80	47	Aug 1996–Dec 2008	NIES	in situ
Key Biscayne, FL, USA	KEY	25.67	−80.20	6.0	Mar 1997–Dec 2008	NOAA CCGG	flask

ACPD
13, 19471–19525, 2013

Table 1b. N_2O measurement site information.

Station	Code	Lat. (° N)	Long. (° E)	Alt. (m a.s.l.)	Data Period Used[1]	Network	Type
Sand Island, USA	MID	28.22	−177.37	4.0	Jul 1997–Dec 2008	NOAA CCGG	flask
Tenerife, Spain	IZO	28.31	−16.48	2377.9	Aug 1995–Dec 2008	NOAA CCGG	flask
WIS Station, Israel	WIS	30.86	34.78	482	Jul 1997–Dec 2008	NOAA CCGG	flask
Moody, TE, USA	WKT	31.31	−97.33	708	Feb 2001–Dec 2008	NOAA CCGG	tower flask
Tudor Hill, Bermuda	BMW	32.26	−64.88	60.0	Jul 1997–Dec 2008	NOAA CCGG	flask
St. Davids Head, UK	BME	32.37	−64.65	17.0	Dec 1995–Dec 2008	NOAA CCGG	flask
Beech Island, SC, USA	SCT	33.41	−81.83	420.0	Aug 2008–Dec 2008	NOAA CCGG	tower flask
Grifton, NC, USA	ITN	35.37	−77.39	505	Mar 1996–Jun 1999	NOAA CCGG	flask
Lampedusa, Italy	LMP	35.51	12.61	50	Oct 2006–Dec 2008	NOAA CCGG	flask
Dwejra Point, Gozo, Malta	GOZ	36.05	14.89	6.0	Jul 1997–Feb 1999	NOAA CCGG	flask
Mt. Waliguan, China	WLG	36.27	100.90	3815	Apr 1997–Dec 2008	NOAA CCGG	flask
Southern Great Plains, OK, USA	SGP	36.60	−97.48	374	Apr 2002–Dec 2008	NOAA CCGG	flask
Tae-ahn Peninsula, South Korea	TAP	36.73	126.13	21.10	Jul 1997–Dec 2008	NOAA CCGG	flask
San Francisco, CA, USA	STR	37.75	−122.45	486	Oct 2007–Dec 2008	NOAA CCGG	tower flask
Walnut Grove, CA, USA	WGC	38.26	−121.49	91	Sep 2007–Dec 2008	NOAA CCGG	tower flask
Terceira Island, Portugal	AZR	38.77	−27.38	24	Oct 1995–Dec 2008	NOAA CCGG	flask
Point Arena, CA, USA	PTA	38.95	−123.74	22.0	Jan 1999–Dec 2008	NOAA CCGG	flask
Wendover, UT, USA	UTA	39.90	−113.72	1332	Dec 1995–Dec 2008	NOAA CCGG	flask
Niwot Ridge, CO, USA	NWR	40.05	−105.58	3526	Jan 1995–Dec 2008	NOAA CCGG&OTTO	flask
					Apr 2002–Dec 2008	NOAA RITS&CATS	in situ
Boulder, CO, USA	BAO	40.05	−105.01	1883.96	Aug 2007–Dec 2008	NOAA CCGG	tower flask
Trinidad Head, California	THD	41.05	−124.15	107	Mar 1995–Dec 2008	AGAGE	in situ
					Apr 2002–Dec 2008	NOAA CCGG&OTTO	flask
Humboldt State University CA, USA	HSU	41.06	−124.75	0.0	May 2008–Oct 2008	NOAA CCGG	flask
Marthas Vineyard, MA, USA	MVY	41.33	−70.52	11.89	Apr 2007–Dec 2008	NOAA CCGG	flask
West Branch, IO, USA	WBI	41.72	−91.35	620.57	Jun 2007–Dec 2008	NOAA CCGG	tower flask
Cape Ochi-ishi, Japan	COI	43.16	145.50	100	Jun 1999–Dec 2008	NIES	in situ
Plateau Assy, Kazakhstan	KZM	43.25	77.88	2524	Oct 1997–Dec 2008	NOAA CCGG	flask
Black Sea, Romania	BSC	44.18	28.67	5.0	Jun 1997–Dec 2008	NOAA CCGG	flask
Sary Taukum, Kazakhstan	KZD	44.45	75.57	412	Oct 1997–Dec 2008	NOAA CCGG	flask
Ulaan Uul, Mongolia	UUM	44.45	111.10	1012	Apr 1997–Dec 2008	NOAA CCGG	flask
Argyle, ME, USA	AMT	45.03	−68.68	157.0	Sep 2003–Dec 2008	NOAA CCGG	tower flask
Cape Meares, OR, USA	CMO	45.48	−123.97	35.0	Jul 1997–Mar 1998	NOAA CCGG	flask
Park Falls, WI, USA	LEF	45.93	−90.27	868	Dec 1005–Dec 2008	NOAA CCGG	flask
Hegyhatsal, Hungary	HUN	46.95	16.65	344	Nov 1995–Dec 2008	NOAA CCGG	flask
Hohenpeissenberg Germany	HPB	47.80	11.02	990.0	Apr 2006–Dec 2008	NOAA CCGG	flask
Estevan Point, Canada	ESP	49.38	−126.53	47.0	Jan 1995–Dec 2008	CSIRO	flask
Ochsenkopf, Finland	OXK	50.03	11.80	1185	Mar 2003–Dec 2008	NOAA CCGG	flask

ACPD
13, 19471–19525, 2013

Table 1c. N_2O measurement site information.

Station	Code	Lat. (° N)	Long. (° E)	Alt.(m a.s.l.)	Data Period Used[1]	Network	Type
Shemya Island, AK, USA	SHM	52.72	174.1	28	Jul 1997–Dec 2008	NOAA CCGG	flask
Mace Head, Ireland	MHD	53.33	−9.90	15	Jan 1995–Dec 2008	AGAGE	in situ
					Apr 1999–Dec 2008	NOAA CCGG&OTTO	flask
Ocean Station M, Norway	STM	66.0	2.0	7.0	Jul 1997–Dec 2008	NOAA CCGG	flask
Lac La Biche, Canada	LLB	54.95	−112.45	546.1	Jan 2008–Dec 2008	NOAA CCGG	flask
Cold Bay, AK, USA	CBA	55.20	−162.72	25.0	Dec 1995–Dec 2008	NOAA CCGG	flask
Baltic Sea, Poland	BAL	55.43	16.95	28.0	Jun 1997–Dec 2008	NOAA CCGG	flask
Shetland Islands, UK	SIS	60.17	−1.17	30.0	Jan 1995–Dec 2008	CSIRO	flask
Surgut, Russia	SUR	61	73	8 levels	Jan 1995–Dec 2008	NIES	flask
Storhofdi, Iceland	ICE	63.25	−20.15	100.0	Jul 1997–Dec 2008	NOAA CCGG	flask
Pallas-Sammaltunturi, Finland	PAL	67.97	24.12	565	Dec 2001–Dec 2008	NOAA CCGG	flask
Pt. Barrow, AK, USA	BRW	71.30	−156.60	11	Jan 1995–Dec 2008	NOAA CCGG&OTTO	flask
					Jan 1995–Dec 2008	NOAA RITS&CATS	in situ
Summit, Greenland	SUM	72.60	−38.40	3214.54	Jun 1997–Dec 2008	NOAA CCGG&OTTO	flask
					Jun 1997–Dec 2008	NOAA CATS	in situ
Mould Bay, Nunavut	MBC	76.25	−119.35	35.0	Jan 1997–May 1997	NOAA CCGG	flask
Ny-Ålesund, Norway	ZEP	78.91	11.88	479	Mar 1997–Dec 2008	NOAA CCGG	flask
Alert, Canada	ALT	82.45	−62.52	205	Jan 1995–Dec 2008	CSIRO	flask
					Nov 1995–Dec 2008	NOAA CCGG&OTTO	flask
South China Sea (3N)	SCSN03	3.00	105.00	20.0	Jul 1997–Oct 1998	NOAA CCGG	flask
South China Sea (6N)	SCSN06	6.00	107.00	20.0	Jul 1997–Oct 1998	NOAA CCGG	flask
South China Sea (9N)	SCSN09	9.00	105.00	20.0	Jul 1997–Oct 1998	NOAA CCGG	flask
South China Sea (12N)	SCSN12	12.00	105.00	20.0	Jul 1997–Oct 1998	NOAA CCGG	flask
South China Sea (15N)	SCSN15	15.00	105.00	20.0	Jul 1997–Oct 1998	NOAA CCGG	flask
South China Sea (18N)	SCSN18	18.00	105.00	20.0	Jul 1997–Oct 1998	NOAA CCGG	flask
South China Sea (21N)	SCSN21	21.00	105.00	20.0	Jul 1997–Oct 1998	NOAA CCGG	flask
Pacific Ocean (0N)	POC000	0.00	−155.00	20.00	Dec 1995–Dec 2008	NOAA CCGG&Tohoku	flask
Pacific Ocean (5N)	POCN05	5.00	−151.00	20.00	Dec 1995–Dec 2008	NOAA CCGG&Tohoku	flask
Pacific Ocean (10N)	POCN10	10.00	−149.00	20.00	Dec 1995–Dec 2008	NOAA CCGG&Tohoku	flask
Pacific Ocean (15N)	POCN15	15.00	−145.00	20.00	Dec 1995–Dec 2008	NOAA CCGG&Tohoku	flask
Pacific Ocean (20N)	POCN20	20.00	−141.00	20.00	Dec 1995–Dec 2008	NOAA CCGG&Tohoku	flask
Pacific Ocean (25N)	POCN25	25.00	−139.00	20.00	Dec 1995–Dec 2008	NOAA CCGG&Tohoku	flask
Pacific Ocean (30N)	POCN30	30.00	−135.00	20.00	Dec 1995–Dec 2008	NOAA CCGG&Tohoku	flask
Pacific Ocean (5S)	POCS05	−5.00	−159.00	20.00	Dec 1995–Dec 2008	NOAA CCGG&Tohoku	flask
Pacific Ocean (10S)	POCS10	−10.00	−161.00	20.00	Dec 1995–Dec 2008	NOAA CCGG&Tohoku	flask
Pacific Ocean (15S)	POCS15	−15.00	−172.00	20.00	Dec 1995–Dec 2008	NOAA CCGG&Tohoku	flask
Pacific Ocean (20S)	POCS20	−20.00	−174.00	20.00	Dec 1995–Dec 2008	NOAA CCGG&Tohoku	flask
Pacific Ocean (25S)	POCS25	−25.00	−171.00	20.00	Dec 1995–Dec 2008	NOAA CCGG&Tohoku	flask
Pacific Ocean (30S)	POCS30	−30.00	−176.00	20.00	Dec 1995–Dec 2008	NOAA CCGG&Tohoku	flask
Pacific Ocean (35S)	POCS35	−35.00	180.00	20.00	Dec 1995–Dec 2008	NOAA CCGG&Tohoku	flask
Western Pacific Cruise	WPC	−30–35	136–170.5	8.0	May 2004–Sep 2008	NOAA CCGG	flask

[1] This is the data period used in our inversion, and some of the records extend before and after the time periods listed.

ACPD
13, 19471–19525, 2013

Table 2. Calibration information among the six measurement networks.

Network	Calibration ratio to AGAGE	measurement error	scale propagation error
AGAGE	1	0.1 %	0.012 %
NOAA CCGG	0.9994	0.1 %	0.07 %
NOAA OTTO&RITS&CATS	1.0009*	0.2 %	0.07 %
NIES	0.9990	0.2 %	0.03 %
CSIRO	0.9989	0.2 %	0.016 %
Tohoku University	1.001	0.3 % before 2002 and 0.1 % since 2002	0.03 %

* Offset values are applied to NOAA OTTO network measurements (1.3 ppb at SMO and 0.6 ppb elsewhere).

ACPD
13, 19471–19525, 2013

Table 3. Prior and optimized global, global land, ocean, and sectoral total N_2O emissions with uncertainties using the GMFD forcing datasets for natural soil emissions prior estimates ($Tg N_2O–N yr^{-1}$)

	Global total		Global land		Ocean		Agricultural Soil		Natural Soil		Industrial		Biomass Burning	
Year	Prior	Posterior	Prior	Posterior	Prior	Posterior	Prior	Posterior	Prior	Posterior	Prior	Posterior	Prior	Posterior
1995	17.63 (±1.87)	13.70 (±0.91)	13.13 (±1.67)	9.69 (±0.79)	4.50 (±0.85)	4.01 (±0.52)	2.96 (±0.52)	2.65 (±0.30)	8.32 (±1.56)	5.27 (±0.65)	1.09 (±0.21)	1.03 (±0.14)	0.76 (±0.18)	0.73 (±0.15)
1996	17.46 (±1.84)	14.28 (±0.77)	12.96 (±1.63)	10.37 (±0.70)	4.50 (±0.85)	3.91 (±0.35)	2.97 (±0.52)	2.74 (±0.31)	8.18 (±1.52)	5.86 (±0.58)	1.08 (±0.20)	1.05 (±0.13)	0.73 (±0.17)	0.72 (±0.13)
1997	16.51 (±1.67)	16.75 (±0.86)	12.01 (±1.44)	11.61 (±0.64)	4.50 (±0.85)	5.14 (±0.61)	2.99 (±0.53)	3.12 (±0.27)	7.24 (±1.32)	6.72 (±0.52)	1.06 (±0.19)	1.05 (±0.11)	0.71 (±0.17)	0.72 (±0.12)
1998	18.30 (±1.98)	15.67 (±0.64)	13.80 (±1.79)	11.07 (±0.57)	4.50 (±0.85)	4.60 (±0.31)	3.01 (±0.53)	3.00 (±0.26)	8.96 (±1.69)	6.30 (±0.46)	1.05 (±0.19)	0.98 (±0.12)	0.78 (±0.17)	0.79 (±0.12)
1999	17.64 (±1.92)	17.26 (±0.66)	13.14 (±1.72)	12.71 (±0.58)	4.50 (±0.85)	4.56 (±0.34)	3.02 (±0.53)	3.30 (±0.28)	8.56 (±1.62)	7.81 (±0.47)	1.03 (±0.19)	1.06 (±0.12)	0.53 (±0.13)	0.54 (±0.10)
2000	17.07 (±1.83)	17.36 (±0.74)	12.57 (±1.62)	12.26 (±0.54)	4.50 (±0.85)	5.10 (±0.50)	3.04 (±0.54)	3.43 (±0.27)	8.05 (±1.52)	7.32 (±0.45)	1.02 (±0.18)	1.03 (±0.11)	0.47 (±0.13)	0.48 (±0.10)
2001	17.38 (±1.88)	18.05 (±0.80)	12.89 (±1.68)	13.46 (±0.61)	4.50 (±0.85)	4.59 (±0.52)	3.08 (±0.54)	3.66 (±0.28)	8.35 (±1.57)	8.26 (±0.52)	1.02 (±0.18)	1.09 (±0.11)	0.43 (±0.12)	0.44 (±0.10)
2002	16.94 (±1.77)	16.97 (±0.68)	12.44 (±1.56)	12.43 (±0.54)	4.50 (±0.85)	4.54 (±0.41)	3.13 (±0.56)	3.51 (±0.28)	7.76 (±1.44)	7.33 (±0.44)	0.97 (±0.17)	0.99 (±0.11)	0.58 (±0.13)	0.60 (±0.10)
2003	17.36 (±1.84)	18.37 (±0.63)	12.86 (±1.63)	13.04 (±0.57)	4.50 (±0.85)	5.33 (±0.26)	3.18 (±0.56)	3.67 (±0.29)	8.08 (±1.51)	7.73 (±0.46)	1.00 (±0.18)	1.01 (±0.11)	0.61 (±0.14)	0.63 (±0.11)
2004	17.02 (±1.77)	17.91 (±0.79)	12.52 (±1.55)	12.21 (±0.52)	4.50 (±0.85)	5.70 (±0.59)	3.26 (±0.58)	3.67 (±0.29)	7.71 (±1.43)	6.94 (±0.41)	1.01 (±0.18)	1.03 (±0.11)	0.55 (±0.12)	0.57 (±0.10)
2005	17.28 (±1.82)	18.71 (±0.65)	12.78 (±1.61)	13.05 (±0.57)	4.50 (±0.85)	5.66 (±0.31)	3.29 (±0.59)	3.56 (±0.31)	7.89 (±1.49)	7.87 (±0.45)	1.02 (±0.18)	1.01 (±0.12)	0.58 (±0.15)	0.61 (±0.12)
2006	17.43 (±1.84)	17.16 (±0.62)	12.93 (±1.64)	12.40 (±0.51)	4.50 (±0.85)	4.76 (±0.35)	3.30 (±0.59)	3.96 (±0.29)	8.04 (±1.51)	6.76 (±0.39)	1.03 (±0.19)	1.09 (±0.11)	0.57 (±0.13)	0.58 (±0.10)
2007	16.95 (±1.78)	19.38 (±0.69)	12.45 (±1.56)	13.85 (±0.48)	4.50 (±0.85)	5.53 (±0.50)	3.30 (±0.59)	3.88 (±0.27)	7.54 (±1.43)	8.28 (±0.37)	1.05 (±0.19)	1.08 (±0.11)	0.57 (±0.13)	0.61 (±0.10)
2008	16.49 (±1.70)	17.83 (±0.71)	11.99 (±1.48)	13.01 (±0.50)	4.50 (±0.85)	4.82 (±0.51)	3.30 (±0.59)	3.92 (±0.27)	7.15 (±1.34)	7.46 (±0.39)	1.07 (±0.19)	1.14 (±0.11)	0.48 (±0.12)	0.49 (±0.09)

ACPD
13, 19471–19525, 2013

Table 4. Prior and optimized regional total N_2O emissions with uncertainties using the GMFD forcing datasets for natural soil emissions prior estimates ($Tg\,N_2O–N\,yr^{-1}$).

	North America		Central/South America		Europe		Africa/Middle East		Northern Asia		Southern Asia		Oceania	
Year	Prior	Posterior	Prior	Posterior	Prior	Posterior	Prior	Posterior	Prior	Posterior	Prior	Posterior	Prior	Posterior
1995	1.29	1.10	2.40	1.77	0.89	0.82	1.77	1.58	2.36	1.45	4.10	2.67	0.31	0.30
	(±0.49)	(±0.36)	(±0.62)	(±0.50)	(±0.44)	(±0.24)	(±0.38)	(±0.33)	(±0.58)	(±0.33)	(±0.96)	(±0.41)	(±0.12)	(±0.12)
1996	1.16	1.09	2.44	1.59	0.85	0.83	1.89	1.73	2.32	1.60	3.94	3.19	0.36	0.35
	(±0.48)	(±0.21)	(±0.60)	(±0.38)	(±0.44)	(±0.31)	(±0.40)	(±0.35)	(±0.56)	(±0.22)	(±0.93)	(±0.36)	(±0.13)	(±0.08)
1997	1.15	1.12	2.40	2.04	0.84	0.82	1.94	1.90	2.04	1.99	3.35	3.46	0.29	0.28
	(±0.47)	(±0.27)	(±0.60)	(±0.41)	(±0.44)	(±0.12)	(±0.40)	(±0.33)	(±0.50)	(±0.23)	(±0.81)	(±0.57)	(±0.11)	(±0.10)
1998	1.23	1.03	2.77	2.58	0.80	0.74	2.00	2.16	2.45	1.06	4.20	3.16	0.35	0.35
	(±0.48)	(±0.15)	(±0.65)	(±0.33)	(±0.44)	(±0.18)	(±0.41)	(±0.32)	(±0.57)	(±0.16)	(±1.01)	(±0.34)	(±0.12)	(±0.08)
1999	1.24	1.32	2.38	2.41	0.78	0.87	1.85	1.92	2.37	2.03	4.18	3.83	0.34	0.33
	(±0.48)	(±0.19)	(±0.56)	(±0.31)	(±0.44)	(±0.11)	(±0.40)	(±0.33)	(±0.57)	(±0.32)	(±1.01)	(±0.27)	(±0.12)	(±0.10)
2000	1.10	1.18	2.32	2.11	0.75	0.80	1.85	2.03	2.43	1.84	3.82	4.01	0.31	0.30
	(±0.47)	(±0.13)	(±0.56)	(±0.33)	(±0.43)	(±0.43)	(±0.38)	(±0.29)	(±0.58)	(±0.23)	(±0.94)	(±0.32)	(±0.11)	(±0.06)
2001	1.14	1.24	2.29	1.98	0.76	0.88	1.84	1.96	2.63	2.80	3.91	4.30	0.32	0.31
	(±0.47)	(±0.45)	(±0.57)	(±0.38)	(±0.44)	(±0.26)	(±0.39)	(±0.34)	(±0.63)	(±0.15)	(±0.95)	(±0.29)	(±0.11)	(±0.07)
2002	1.15	1.19	2.59	3.01	0.76	0.81	1.81	2.08	2.36	1.30	3.49	3.77	0.28	0.28
	(±0.47)	(±0.27)	(±0.61)	(±0.31)	(±0.44)	(±0.12)	(±0.37)	(±0.29)	(±0.56)	(±0.22)	(±0.85)	(±0.38)	(±0.11)	(±0.11)
2003	1.17	1.18	2.42	2.82	0.74	0.79	1.95	2.31	2.39	1.81	3.92	3.84	0.29	0.29
	(±0.48)	(±0.14)	(±0.57)	(±0.34)	(±0.43)	(±0.22)	(±0.41)	(±0.34)	(±0.56)	(±0.16)	(±0.94)	(±0.25)	(±0.11)	(±0.10)
2004	1.22	1.16	2.46	2.85	0.77	0.80	1.78	1.97	2.22	1.52	3.73	3.58	0.34	0.33
	(±0.48)	(±0.23)	(±0.57)	(±0.34)	(±0.44)	(±0.09)	(±0.36)	(±0.29)	(±0.54)	(±0.21)	(±0.89)	(±0.56)	(±0.12)	(±0.10)
2005	1.21	1.10	2.44	2.49	0.76	0.74	1.85	2.04	2.21	1.65	4.02	4.74	0.29	0.29
	(±0.48)	(±0.11)	(±0.55)	(±0.33)	(±0.43)	(±0.21)	(±0.38)	(±0.30)	(±0.54)	(±0.17)	(±0.96)	(±0.37)	(±0.11)	(±0.10)
2006	1.14	1.25	2.51	2.95	0.77	0.85	1.87	2.14	2.23	0.73	4.06	4.12	0.36	0.36
	(±0.47)	(±0.20)	(±0.58)	(±0.30)	(±0.44)	(±0.10)	(±0.38)	(±0.30)	(±0.54)	(±0.29)	(±0.95)	(±0.25)	(±0.12)	(±0.09)
2007	1.11	1.17	2.11	2.22	0.77	0.81	1.83	2.20	2.40	1.77	3.95	5.40	0.28	0.27
	(±0.47)	(±0.10)	(±0.44)	(±0.24)	(±0.44)	(±0.43)	(±0.37)	(±0.27)	(±0.58)	(±0.21)	(±0.94)	(±0.33)	(±0.11)	(±0.09)
2008	1.09	1.25	2.11	2.49	0.76	0.86	1.77	1.94	2.37	2.57	3.61	3.63	0.27	0.27
	(±0.47)	(±0.44)	(±0.46)	(±0.26)	(±0.44)	(±0.24)	(±0.36)	(±0.30)	(±0.57)	(±0.17)	(±0.87)	(±0.26)	(±0.12)	(±0.12)

ACPD
13, 19471–19525, 2013

Table 5. Prior and optimized regional agricultural soil N_2O emissions with uncertainties using the GMFD forcing datasets for natural soil emissions prior estimates ($GgN_2O–N\,yr^{-1}$).

	North America		Central/South America		Europe		Africa/Middle East		Northern Asia		Southern Asia		Oceania	
Year	Prior	Posterior	Prior	Posterior	Prior	Posterior	Prior	Posterior	Prior	Posterior	Prior	Posterior	Prior	Posterior
1995	392.79	363.49	384.31	358.63	352.78	324.08	374.48	354.03	392.02	359.16	984.61	816.27	77.17	75.98
	(±60.96)	(±54.37)	(±58.35)	(±57.45)	(±49.17)	(±33.39)	(±55.41)	(±53.81)	(±60.72)	(±52.21)	(±383.04)	(±120.60)	(± 2.35)	(± 2.08)
1996	395.51	387.79	388.49	357.55	348.97	342.89	383.18	371.68	388.78	365.37	990.30	841.69	78.93	74.85
	(±61.80)	(±53.85)	(±59.63)	(±58.07)	(±48.11)	(±33.84)	(±58.01)	(±56.26)	(±59.72)	(±52.65)	(±387.48)	(±145.91)	(± 2.46)	(± 2.07)
1997	398.23	408.88	392.68	367.16	345.16	331.92	391.89	399.97	385.55	394.23	995.99	1139.68	80.68	79.31
	(±62.66)	(±41.57)	(±60.92)	(±58.07)	(±47.07)	(±22.90)	(±60.68)	(±54.42)	(±58.73)	(±41.51)	(±391.94)	(±107.57)	(± 2.57)	(± 2.03)
1998	400.95	369.94	396.86	393.36	341.35	310.60	400.60	420.58	382.31	363.97	1001.68	1061.94	82.44	80.05
	(±63.52)	(±36.07)	(±62.23)	(±59.16)	(±46.04)	(±21.42)	(±63.40)	(±51.58)	(±57.75)	(±32.52)	(±396.43)	(±90.28)	(± 2.69)	(± 2.10)
1999	403.67	459.27	401.05	384.37	337.54	385.36	409.30	436.87	379.08	398.64	1007.37	1150.01	84.19	81.87
	(±64.38)	(±41.80)	(±63.55)	(±58.50)	(±45.01)	(±21.12)	(±66.19)	(±55.24)	(±56.78)	(±36.52)	(±400.95)	(±98.83)	(± 2.80)	(± 2.58)
2000	406.39	471.47	405.23	382.81	333.73	361.75	418.01	459.64	375.84	394.50	1013.06	1273.47	85.95	81.87
	(±65.25)	(±39.82)	(±64.88)	(±61.48)	(±44.00)	(±19.16)	(±69.04)	(±55.02)	(±55.81)	(±33.80)	(±405.49)	(±95.08)	(± 2.92)	(± 2.60)
2001	410.88	497.40	420.97	396.85	335.24	403.08	427.37	475.16	377.27	434.49	1023.52	1373.93	86.53	81.39
	(±66.70)	(±31.06)	(±70.02)	(±66.40)	(±44.40)	(±18.78)	(±72.17)	(±56.56)	(±56.24)	(±35.23)	(±413.91)	(±107.98)	(± 2.96)	(± 2.69)
2002	405.93	450.03	435.23	449.76	331.20	357.55	438.24	494.46	379.15	394.53	1059.72	1284.53	83.56	82.14
	(±65.10)	(±21.93)	(±74.84)	(±70.29)	(±43.34)	(±18.88)	(±75.88)	(±60.16)	(±56.80)	(±37.33)	(±443.71)	(±122.52)	(± 2.76)	(± 2.55)
2003	416.95	466.86	470.95	486.55	326.35	351.76	439.54	505.00	378.27	399.38	1063.99	1377.80	82.56	80.61
	(±68.69)	(±16.22)	(±87.63)	(±79.93)	(±42.08)	(±17.98)	(±76.33)	(±59.66)	(±56.54)	(±36.75)	(±447.28)	(±133.95)	(± 2.69)	(± 2.44)
2004	426.63	465.61	475.54	477.69	331.82	346.99	448.24	498.14	383.50	398.47	1104.59	1403.43	85.87	83.91
	(±71.91)	(±17.93)	(±89.35)	(±80.13)	(±43.50)	(±20.01)	(±79.38)	(±60.44)	(±58.11)	(±39.12)	(±482.07)	(±132.02)	(± 2.91)	(± 2.50)
2005	427.76	432.88	488.15	491.36	327.85	320.00	456.09	494.51	386.30	387.96	1119.44	1350.60	87.41	84.44
	(±72.29)	(±19.93)	(±94.15)	(±80.34)	(±42.47)	(±19.50)	(±82.19)	(±61.88)	(±58.96)	(±38.45)	(±495.12)	(±155.89)	(± 3.02)	(± 2.47)
2006	428.06	500.45	488.49	483.20	328.08	366.60	456.41	522.35	386.57	418.95	1120.22	1583.04	87.47	86.86
	(±72.40)	(±19.97)	(±94.28)	(±83.59)	(±42.53)	(±18.35)	(±82.30)	(±59.73)	(±59.04)	(±37.56)	(±495.81)	(±127.01)	(± 3.02)	(± 2.66)
2007	428.36	489.18	488.83	489.72	328.31	350.96	456.73	527.27	386.84	408.25	1121.00	1527.85	87.53	83.18
	(±72.50)	(±17.66)	(±94.41)	(±74.55)	(±42.59)	(±19.23)	(±82.42)	(±58.36)	(±59.12)	(±35.89)	(±496.50)	(±128.34)	(± 3.03)	(± 2.44)
2008	428.66	544.76	489.18	503.00	328.54	378.19	457.05	509.63	387.11	427.15	1121.79	1468.41	87.59	86.89
	(±72.60)	(±15.13)	(±94.54)	(±76.66)	(±42.65)	(±19.42)	(±82.53)	(±60.00)	(±59.21)	(±35.31)	(±497.20)	(±134.40)	(± 3.03)	(± 2.48)

ACPD
13, 19471–19525, 2013

Table 6. Prior and optimized regional industrial N_2O emissions with uncertainties using the GMFD forcing datasets for natural soil emissions prior estimates ($GgN_2O–N\,yr^{-1}$).

	North America		Central/South America		Europe		Africa/Middle East		Northern Asia		Southern Asia		Oceania	
Year	Prior	Posterior	Prior	Posterior	Prior	Posterior	Prior	Posterior	Prior	Posterior	Prior	Posterior	Prior	Posterior
1995	212.15	203.51	33.87	33.67	353.20	321.71	69.23	68.54	196.83	188.03	222.48	214.08	4.93	4.93
	(±17.78)	(±17.19)	(± 0.45)	(± 0.45)	(±49.29)	(±34.69)	(± 1.89)	(± 1.89)	(±15.31)	(±14.58)	(±19.56)	(±17.08)	(± 0.01)	(± 0.01)
1996	209.14	207.47	34.74	34.49	327.90	320.77	70.48	70.12	203.89	198.12	225.85	215.74	5.21	5.19
	(±17.28)	(±16.58)	(± 0.48)	(± 0.48)	(±42.48)	(±31.17)	(± 1.96)	(± 1.96)	(±16.42)	(±15.59)	(±20.15)	(±17.04)	(± 0.01)	(± 0.01)
1997	206.13	200.92	35.61	35.40	302.61	296.73	71.73	72.03	210.94	195.43	229.21	239.43	5.49	5.48
	(±16.79)	(±13.85)	(± 0.50)	(± 0.50)	(±36.18)	(±22.01)	(± 2.03)	(± 2.02)	(±17.58)	(± 7.83)	(±20.76)	(±17.44)	(± 0.01)	(± 0.01)
1998	203.12	185.80	36.47	36.46	277.31	261.27	72.98	73.64	217.99	186.12	232.58	232.69	5.76	5.75
	(±16.30)	(±12.65)	(± 0.53)	(± 0.53)	(±30.38)	(±17.98)	(± 2.10)	(± 2.07)	(±18.77)	(± 7.87)	(±21.37)	(±17.58)	(± 0.01)	(± 0.01)
1999	200.11	208.66	37.34	37.20	252.02	281.30	74.24	75.38	225.04	214.73	235.95	234.36	6.04	6.03
	(±15.82)	(±11.03)	(± 0.55)	(± 0.55)	(±25.09)	(±16.24)	(± 2.18)	(± 2.15)	(±20.01)	(± 9.43)	(±22.00)	(±19.02)	(± 0.01)	(± 0.01)
2000	197.10	205.29	38.21	38.03	226.73	242.84	75.49	77.11	232.09	219.39	239.32	245.49	6.32	6.30
	(±15.35)	(±10.42)	(± 0.58)	(± 0.58)	(±20.31)	(±13.85)	(± 2.25)	(± 2.20)	(±21.28)	(± 8.80)	(±22.63)	(±19.07)	(± 0.02)	(± 0.02)
2001	183.93	198.91	38.78	38.61	236.17	271.34	75.65	77.57	230.97	238.55	244.16	263.13	6.15	6.13
	(±13.37)	(± 9.44)	(± 0.59)	(± 0.59)	(±22.04)	(±13.85)	(± 2.26)	(± 2.22)	(±21.08)	(± 8.56)	(±23.55)	(±20.03)	(± 0.01)	(± 0.01)
2002	180.49	186.49	38.73	38.87	228.99	243.13	75.47	77.35	203.01	192.48	239.57	246.63	5.86	5.85
	(±12.87)	(± 8.48)	(± 0.59)	(± 0.59)	(±20.72)	(±13.40)	(± 2.25)	(± 2.22)	(±16.28)	(± 7.03)	(±22.68)	(±20.79)	(± 0.01)	(± 0.01)
2003	176.93	179.20	39.43	39.57	240.11	257.74	79.04	81.42	206.90	189.53	250.23	257.90	6.47	6.45
	(±12.37)	(± 8.23)	(± 0.61)	(± 0.61)	(±22.78)	(±14.27)	(± 2.47)	(± 2.42)	(±16.91)	(± 6.93)	(±24.74)	(±21.35)	(± 0.02)	(± 0.02)
2004	174.25	174.33	40.57	40.61	247.50	259.93	78.60	80.33	208.02	197.77	250.86	265.54	6.70	6.69
	(±12.00)	(± 8.49)	(± 0.65)	(± 0.65)	(±24.20)	(±15.19)	(± 2.44)	(± 2.40)	(±17.10)	(± 7.78)	(±24.86)	(±21.31)	(± 0.02)	(± 0.02)
2005	171.79	169.85	41.35	41.39	247.65	243.61	80.97	82.27	208.18	191.99	259.68	270.89	7.08	7.06
	(±11.66)	(± 8.34)	(± 0.68)	(± 0.67)	(±24.23)	(±14.93)	(± 2.59)	(± 2.54)	(±17.12)	(± 8.52)	(±26.64)	(±22.49)	(± 0.02)	(± 0.02)
2006	174.57	184.20	42.02	42.01	251.67	278.36	82.29	84.77	211.56	210.04	263.89	286.29	7.19	7.18
	(±12.04)	(± 8.39)	(± 0.70)	(± 0.70)	(±25.02)	(±14.72)	(± 2.68)	(± 2.62)	(±17.68)	(± 8.28)	(±27.51)	(±23.19)	(± 0.02)	(± 0.02)
2007	177.40	185.83	42.70	42.74	255.74	271.40	83.62	86.17	214.98	208.17	268.16	281.83	7.31	7.28
	(±12.43)	(± 7.92)	(± 0.72)	(± 0.72)	(±25.84)	(±14.63)	(± 2.76)	(± 2.69)	(±18.26)	(± 7.27)	(±28.41)	(±23.20)	(± 0.02)	(± 0.02)
2008	180.28	198.71	43.39	43.53	259.89	292.97	84.97	87.12	218.47	222.54	272.50	285.39	7.43	7.42
	(±12.84)	(± 7.82)	(± 0.74)	(± 0.74)	(±26.69)	(±15.54)	(± 2.85)	(± 2.78)	(±18.86)	(± 8.48)	(±29.34)	(±24.59)	(± 0.02)	(± 0.02)

ACPD
13, 19471–19525, 2013

Table 7. Prior and optimized regional natural soil N_2O emissions with uncertainties using the GMFD forcing datasets for natural soil emissions prior estimates ($GgN_2O–N\,yr^{-1}$).

	North America		Central/South America		Europe		Africa/Middle East		Northern Asia		Southern Asia		Oceania	
Year	Prior	Posterior	Prior	Posterior	Prior	Posterior	Prior	Posterior	Prior	Posterior	Prior	Posterior	Prior	Posterior
1995	679.29 (±182.31)	520.96 (±111.37)	1919.51 (±1455.75)	1317.35 (±787.31)	183.39 (± 13.29)	170.51 (± 12.58)	955.68 (±360.86)	803.51 (±297.47)	1728.21 (±1180.06)	860.72 (±174.41)	2661.23 (±2798.17)	1411.52 (±230.81)	193.88 (± 14.85)	187.61 (± 12.94)
1996	543.66 (±116.78)	488.32 (± 62.05)	1952.74 (±1506.60)	1133.15 (±478.70)	172.38 (± 11.74)	166.74 (± 11.11)	1077.90 (±459.05)	935.31 (±363.08)	1682.49 (±1118.44)	992.80 (± 90.03)	2498.97 (±2467.36)	1908.48 (±389.85)	247.64 (± 24.23)	233.06 (± 19.68)
1997	533.19 (±112.32)	500.88 (± 47.20)	1914.88 (±1448.75)	1576.37 (±519.88)	192.10 (± 14.58)	187.74 (± 7.93)	1121.76 (±497.18)	1078.62 (±308.63)	1407.43 (±782.64)	1356.34 (± 68.90)	1905.82 (±1435.07)	1858.94 (±148.61)	169.08 (± 11.30)	165.74 (± 9.62)
1998	583.93 (±134.72)	431.03 (± 46.18)	2200.40 (±1912.99)	2009.65 (±375.06)	182.21 (± 13.12)	168.23 (± 7.83)	1158.40 (±530.18)	1278.65 (±308.87)	1725.19 (±1175.94)	405.67 (± 69.42)	2875.57 (±3267.06)	1774.09 (±115.77)	235.18 (± 21.85)	231.11 (± 16.99)
1999	619.21 (±151.49)	631.09 (± 50.07)	1855.17 (±1359.80)	1904.05 (±322.15)	189.12 (± 14.13)	201.22 (± 8.49)	1065.73 (±448.75)	1102.70 (±276.49)	1729.30 (±1181.54)	1377.06 (±101.97)	2889.03 (±3297.72)	2390.58 (±199.19)	210.43 (± 17.49)	206.50 (± 16.27)
2000	488.51 (± 94.29)	486.87 (± 31.69)	1835.96 (±1331.78)	1641.93 (±323.00)	184.59 (± 13.46)	192.31 (± 8.82)	1048.75 (±434.56)	1179.98 (±267.97)	1761.80 (±1226.37)	1172.18 (± 73.04)	2550.00 (±2569.14)	2470.85 (±112.20)	180.65 (± 12.89)	173.50 (± 10.99)
2001	537.48 (±114.14)	534.25 (± 38.08)	1790.40 (±1266.51)	1511.35 (±394.32)	188.33 (± 14.01)	201.45 (± 8.54)	1054.77 (±439.57)	1108.06 (±307.50)	1981.75 (±1551.69)	2089.96 (± 42.55)	2620.00 (±2712.14)	2637.61 (±237.84)	181.36 (± 13.00)	174.93 (± 12.16)
2002	526.63 (±109.58)	515.63 (± 32.37)	2040.23 (±1644.63)	2438.69 (±302.39)	198.86 (± 15.62)	203.14 (± 7.84)	1004.89 (±398.97)	1199.51 (±265.79)	1698.17 (±1139.38)	637.77 (± 45.25)	2128.59 (±1790.17)	2170.24 (±209.06)	161.68 (± 10.33)	160.84 (± 9.69)
2003	538.01 (±114.37)	502.39 (± 29.26)	1828.63 (±1321.17)	2217.43 (±314.39)	171.15 (± 11.57)	174.31 (± 6.26)	1130.62 (±505.06)	1400.09 (±293.53)	1664.21 (±1094.27)	1083.86 (± 79.11)	2559.41 (±2588.15)	2162.93 (±133.42)	184.65 (± 13.47)	184.14 (± 12.86)
2004	575.77 (±130.98)	478.34 (± 24.10)	1841.38 (±1339.66)	2222.21 (±324.44)	187.39 (± 13.87)	187.74 (± 6.67)	973.61 (±374.53)	1103.70 (±229.77)	1617.60 (±1033.83)	908.24 (± 40.84)	2308.74 (±2106.00)	1835.80 (± 86.98)	203.97 (± 16.44)	203.96 (± 15.37)
2005	580.68 (±133.22)	470.45 (± 27.21)	1764.26 (±1229.80)	1811.49 (±285.14)	180.02 (± 12.80)	174.63 (± 5.76)	984.32 (±382.81)	1107.66 (±253.20)	1594.23 (±1004.17)	1047.86 (± 84.73)	2604.91 (±2680.99)	3080.32 (±201.06)	177.26 (± 12.41)	176.13 (± 11.64)
2006	510.65 (±103.03)	539.34 (± 23.35)	1911.59 (±1443.78)	2358.14 (±232.65)	191.30 (± 14.46)	209.05 (± 6.69)	1034.90 (±423.16)	1221.51 (±233.58)	1582.08 (±988.93)	49.64 (± 20.44)	2582.92 (±2635.92)	2158.76 (±115.70)	225.55 (± 20.10)	227.63 (± 18.77)
2007	490.94 (± 95.23)	485.56 (± 17.82)	1423.59 (±800.71)	1519.80 (±169.82)	185.84 (± 13.65)	190.05 (± 7.79)	1004.34 (±398.54)	1276.18 (±247.99)	1774.55 (±1244.18)	1126.14 (± 38.93)	2502.80 (±2474.93)	3529.06 (±156.02)	155.95 (± 9.61)	153.27 (± 9.02)
2008	450.18 (± 80.07)	473.48 (± 17.50)	1520.81 (±913.81)	1885.11 (±214.95)	174.95 (± 12.09)	186.70 (± 7.00)	942.36 (±350.87)	1040.22 (±238.10)	1711.16 (±1156.88)	1861.16 (± 87.33)	2196.15 (±1905.61)	1855.38 (±147.80)	156.60 (± 9.69)	158.11 (± 9.22)

ACPD
13, 19471–19525, 2013

Table 8. Prior and optimized regional ocean N_2O emissions with uncertainties using the GMFD forcing datasets for natural soil emissions prior estimates ($GgN_2O–N\,yr^{-1}$)

	North Pacific		South Pacific		Northern Ocean		Atlantic		Southern Ocean		Indian Ocean	
Year	Prior	Posterior	Prior	Posterior	Prior	Posterior	Prior	Posterior	Prior	Posterior	Prior	Posterior
1995	324.27 (± 41.55)	338.94 (± 11.51)	1292.88 (±660.43)	1112.76 (±341.22)	95.58 (± 3.61)	0.10 (± 3.09)	663.28 (±173.82)	636.31 (±136.06)	1040.35 (±427.63)	890.04 (±106.10)	1082.73 (±463.18)	934.14 (±327.09)
1996	324.58 (± 41.62)	324.58 (± 41.62)	1292.83 (±660.38)	1134.66 (± 7.86)	95.57 (± 3.61)	0.09 (± 3.58)	663.32 (±173.84)	645.87 (± 22.44)	1040.09 (±427.42)	982.54 (±303.34)	1082.70 (±463.15)	727.14 (± 51.60)
1997	324.27 (± 41.55)	305.83 (± 39.35)	1292.88 (±660.43)	1292.88 (±660.43)	95.58 (± 3.61)	0.10 (± 2.29)	663.28 (±173.82)	648.54 (±119.53)	1040.35 (±427.63)	1531.11 (± 11.68)	1082.73 (±463.18)	1265.91 (±209.92)
1998	324.27 (± 41.55)	276.69 (± 22.73)	1292.88 (±660.43)	1016.05 (±174.74)	95.58 (± 3.61)	0.10 (± 3.61)	663.28 (±173.82)	713.77 (± 7.54)	1040.35 (±427.63)	1185.05 (±123.07)	1082.73 (±463.18)	1311.26 (± 6.03)
1999	324.27 (± 41.55)	337.82 (± 31.99)	1292.88 (±660.43)	950.23 (± 22.02)	95.58 (± 3.61)	0.10 (± 3.56)	663.28 (±173.82)	663.28 (±173.82)	1040.35 (±427.63)	1316.23 (± 6.28)	1082.73 (±463.18)	1194.55 (± 74.71)
2000	324.58 (± 41.62)	392.74 (± 7.87)	1292.83 (±660.38)	1698.95 (±140.72)	95.57 (± 3.61)	0.09 (± 3.31)	663.32 (±173.84)	621.47 (± 83.17)	1040.09 (±427.42)	1040.09 (±427.42)	1082.70 (±463.15)	1252.56 (± 6.27)
2001	324.27 (± 41.55)	329.53 (± 32.87)	1292.88 (±660.43)	1746.01 (± 5.38)	95.58 (± 3.61)	0.10 (± 3.55)	663.28 (±173.82)	414.29 (± 32.90)	1040.35 (±427.63)	918.55 (±172.38)	1082.73 (±463.18)	1082.73 (±463.18)
2002	324.27 (± 41.55)	500.78 (± 4.01)	1292.88 (±660.43)	1439.90 (±188.64)	95.58 (± 3.61)	0.12 (± 2.54)	663.28 (±173.82)	963.64 (± 80.83)	1040.35 (±427.63)	591.44 (± 36.65)	1082.73 (±463.18)	933.85 (±173.08)
2003	324.27 (± 41.55)	324.27 (± 41.55)	1292.88 (±660.43)	1527.26 (± 6.08)	95.58 (± 3.61)	0.10 (± 3.54)	663.28 (±173.82)	968.09 (± 8.30)	1040.35 (±427.63)	1439.36 (±114.03)	1082.73 (±463.18)	976.69 (± 26.80)
2004	324.58 (± 41.62)	339.27 (± 35.72)	1292.83 (±660.38)	1292.83 (±660.38)	95.57 (± 3.61)	0.11 (± 2.07)	663.32 (±173.84)	803.58 (± 65.23)	1040.09 (±427.42)	1606.99 (± 8.09)	1082.70 (±463.15)	1555.40 (±115.57)
2005	324.27 (± 41.55)	296.94 (± 21.56)	1292.88 (±660.43)	1419.40 (±148.92)	95.58 (± 3.61)	0.10 (± 3.61)	663.28 (±173.82)	979.85 (± 4.34)	1040.35 (±427.63)	1265.38 (± 85.95)	1082.73 (±463.18)	1599.92 (± 5.92)
2006	324.27 (± 41.55)	362.03 (± 32.49)	1292.88 (±660.43)	937.96 (± 19.03)	95.58 (± 3.61)	0.10 (± 3.55)	663.28 (±173.82)	663.28 (±173.82)	1040.35 (±427.63)	1428.51 (± 4.53)	1082.73 (±463.18)	1273.52 (± 73.11)
2007	324.27 (± 41.55)	371.84 (± 7.09)	1292.88 (±660.43)	1674.28 (±130.95)	95.58 (± 3.61)	0.09 (± 3.23)	663.28 (±173.82)	651.53 (± 71.32)	1040.35 (±427.63)	1040.35 (±427.63)	1082.73 (±463.18)	1695.89 (± 4.21)
2008	324.58 (± 41.62)	349.10 (± 28.20)	1292.83 (±660.38)	1784.24 (± 5.45)	95.57 (± 3.61)	0.10 (± 3.54)	663.32 (±173.84)	489.98 (± 26.26)	1040.09 (±427.42)	1019.83 (±140.88)	1082.70 (±463.15)	1082.70 (±463.15)

ACPD
13, 19471–19525, 2013

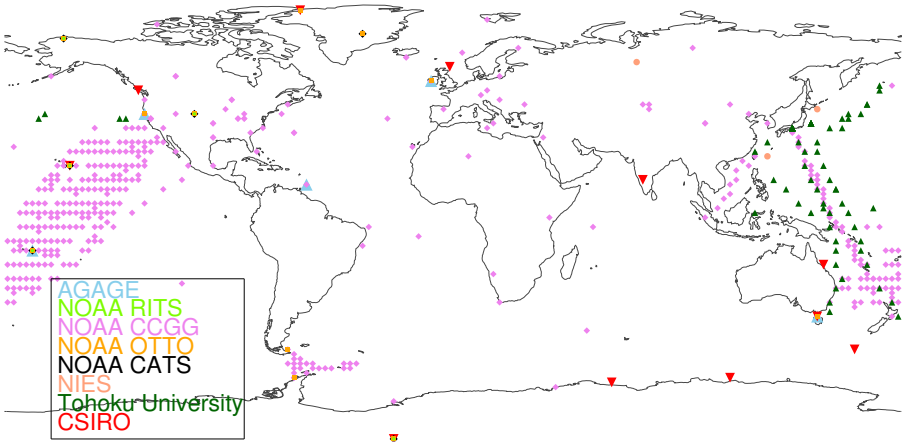

Fig. 1. Sampling networks and locations for the measurements used in the N_2O inversions. See also Table 1.

ACPD
13, 19471–19525, 2013

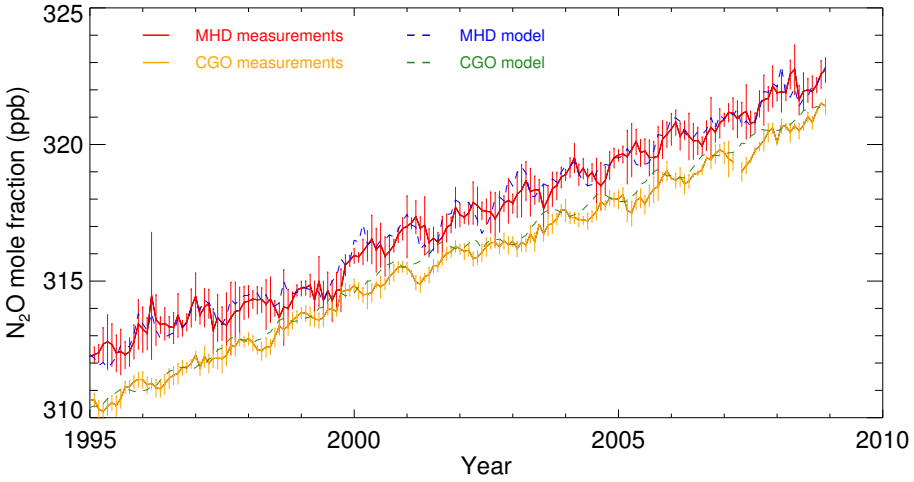

Fig. 2. Combined N_2O observations at Cape Grim, Tasmania (CGO, orange) and Mace Head, Ireland (MHD, red) from AGAGE and NOAA networks. Atmospheric mole fractions predicted by MOZART v4 using optimized emissions with GMFD prior emissions estimates for natural soil are shown in dashed lines for CGO (green) and MHD (blue).

ACPD
13, 19471–19525, 2013

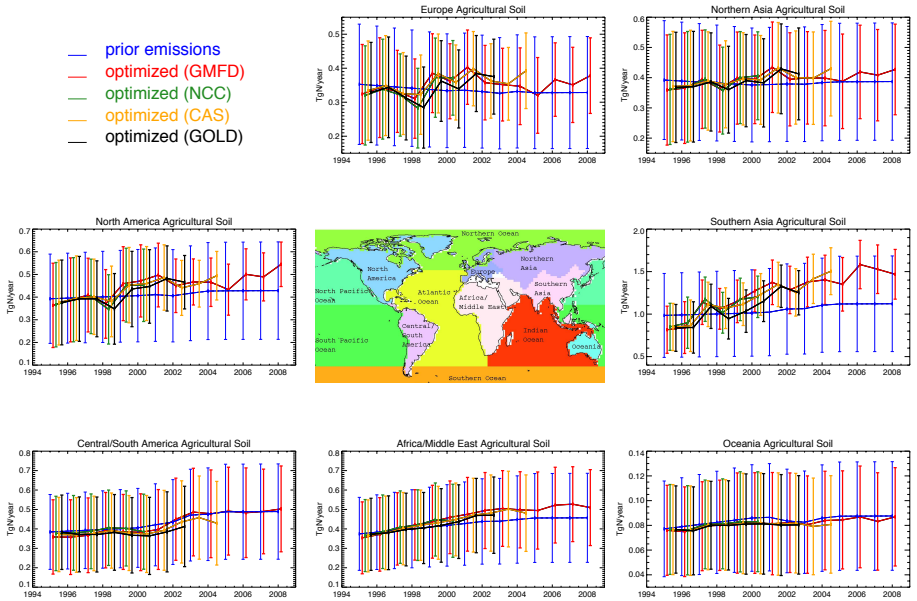

Fig. 3a. Comparison of prior (blue) and optimized agricultural soil emissions in $Tg\,N_2O–N\,yr^{-1}$ from four inversions for seven regions, each using a different forcing dataset for natural soil (red: GMFD; green: NCC; orange: CAS; and black: GOLD). Prior emissions uncertainties are 40 %, and posterior uncertainties are one standard deviation.

ACPD
13, 19471–19525, 2013

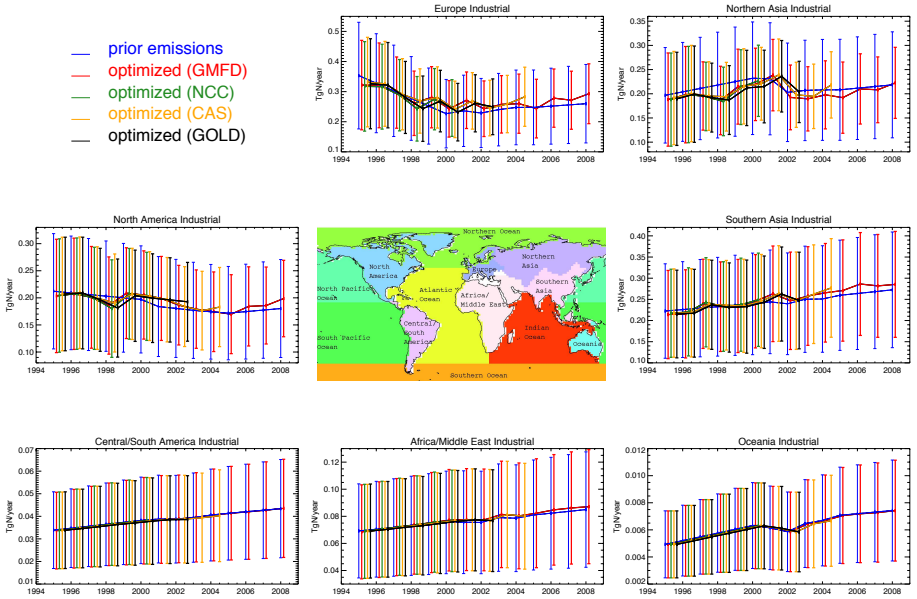

Fig. 3b. Comparison of prior (blue) and optimized industrial emissions in $Tg\,N_2O–N\,yr^{-1}$ from four inversions for seven regions, each using a different forcing dataset for natural soil (red: GMFD; green: NCC; orange: CAS; and black: GOLD). Prior emissions uncertainties are 40 %, and posterior uncertainties are one standard deviation.

ACPD
13, 19471–19525, 2013

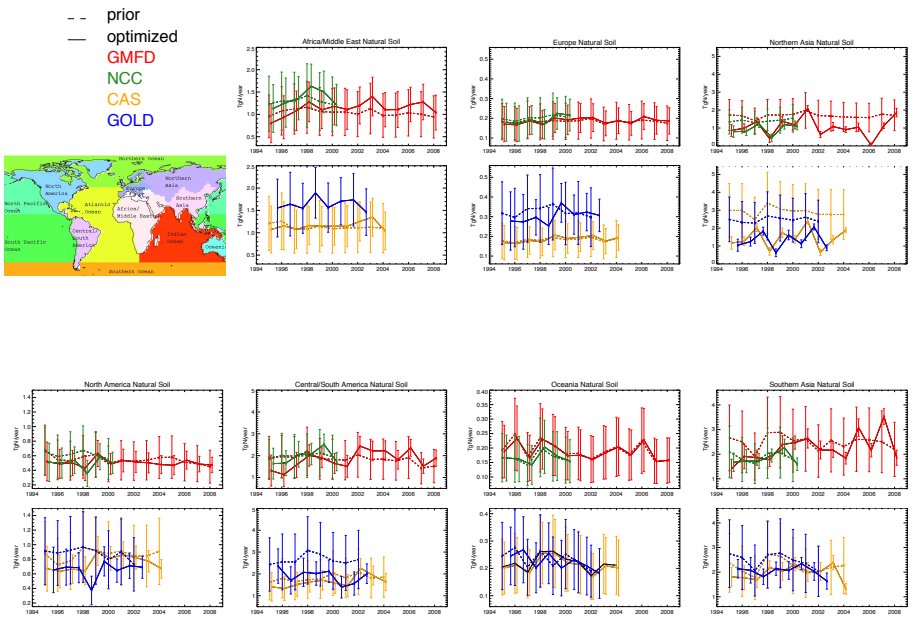

Fig. 3c. Comparison of prior (dash) and optimized (solid) natural soil emissions in $Tg\,N_2O–N\,yr^{-1}$ from four inversions for seven regions, each using a different forcing dataset for natural soil (red: GMFD; green: NCC; orange: CAS; and blue: GOLD). Prior emissions uncertainties are 40 %, and posterior uncertainties are one standard deviation.

ACPD
13, 19471–19525, 2013

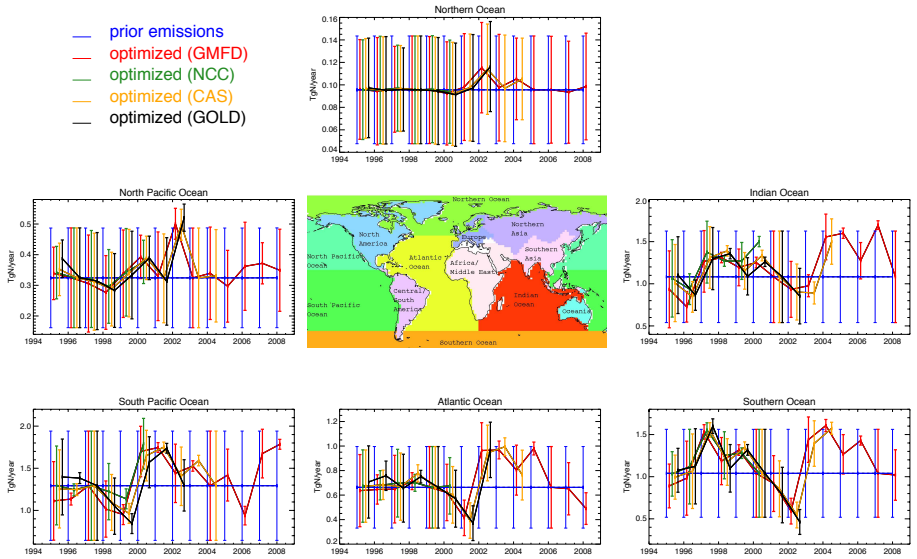

Fig. 3d. Comparison of prior (blue) and optimized ocean emissions in $Tg\,N_2O–N\,yr^{-1}$ from four inversions for six regions, each using a different forcing dataset for natural soil (red: GMFD; green: NCC; orange: CAS; and black: GOLD). Prior emissions uncertainties are 40 %, and posterior uncertainties are one standard deviation.

ACPD
13, 19471–19525, 2013

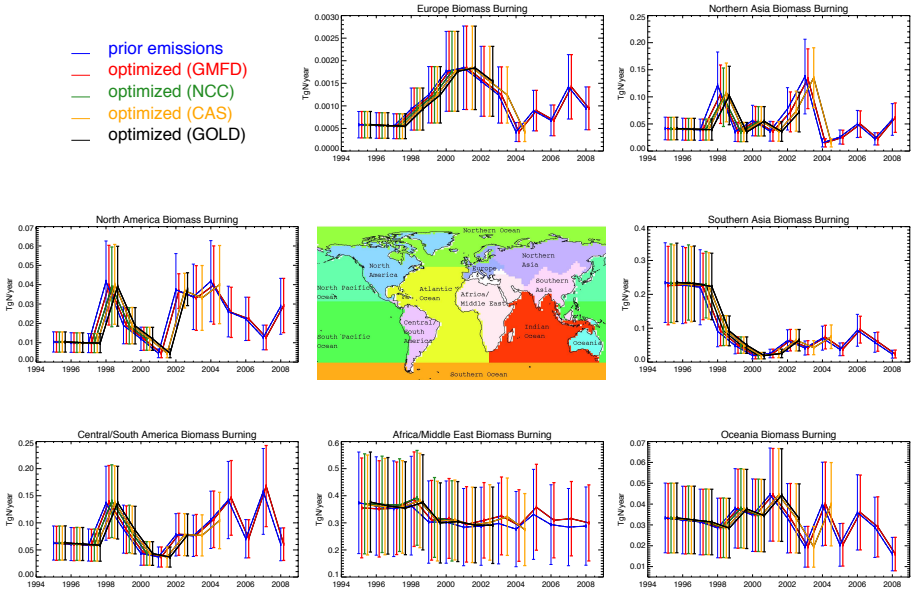

Fig. 3e. Comparison of prior (blue) and optimized biomass burning emissions in Tg N_2O–N yr^{-1} from four inversions for seven regions, each using a different set forcing dataset for natural soil (red: GMFD; green: NCC; orange: CAS; and black: GOLD). Prior emissions uncertainties are 40 %, and posterior uncertainties are one standard deviation.

ACPD
13, 19471–19525, 2013

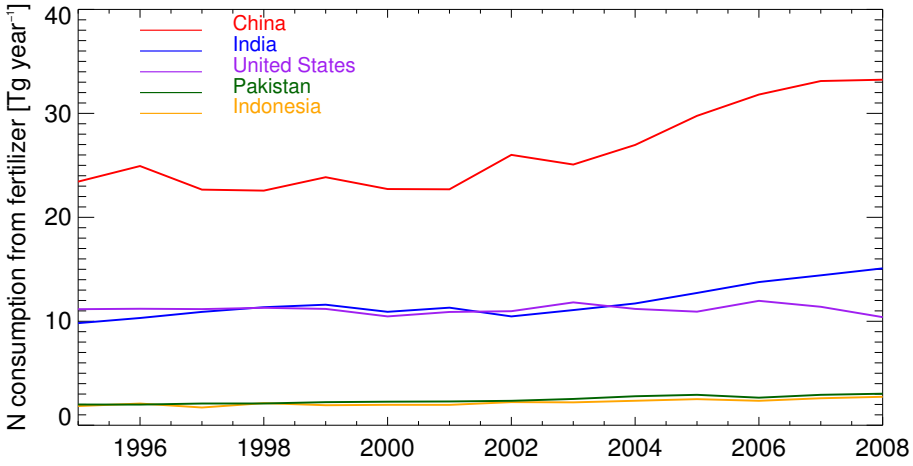

Fig. 4. Changes in nitrogen consumption from fertilizers by the top five consumers in the world in Tg N yr^{-1} (International Fertilizer Industry Association).

ACPD
13, 19471–19525, 2013

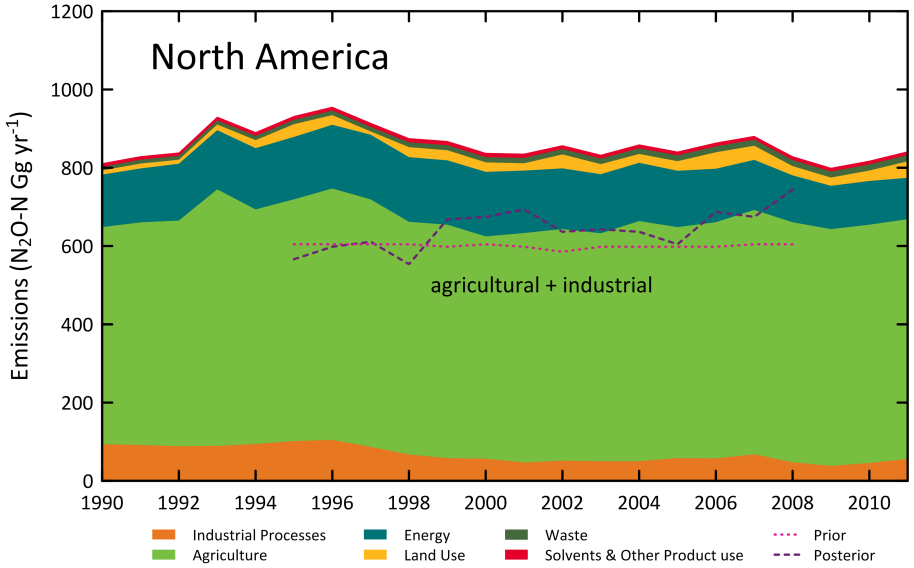

Fig. 5a. Comparison of IPCC estimates with our prior (pink dot) and optimized agricultural and industrial emissions (purple dash) in Gg N_2O–N yr^{-1} for North America.

ACPD
13, 19471–19525, 2013

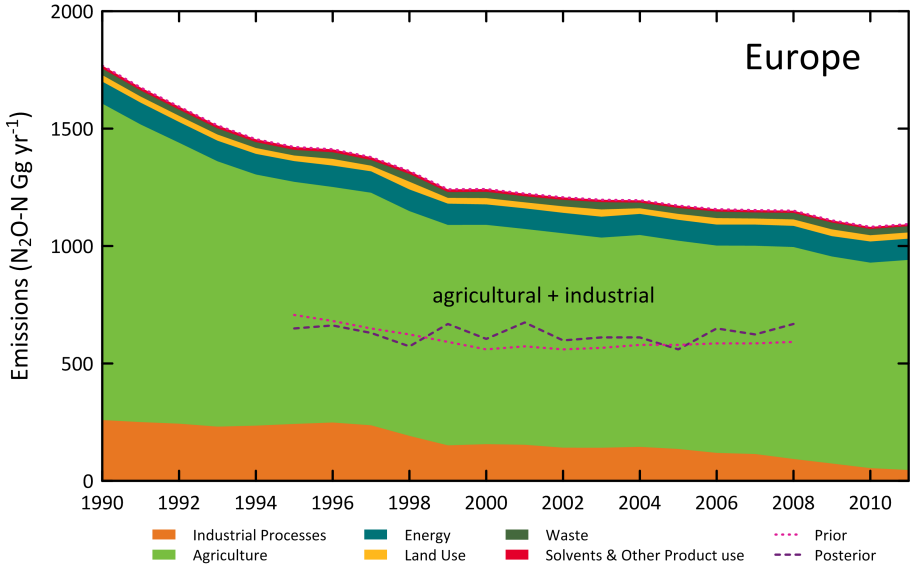

Fig. 5b. Comparison of IPCC estimates with our prior (pink dot) and optimized agricultural and industrial emissions (purple dash) in Gg N_2O–N yr^{-1} for Europe.

ACPD
13, 19471–19525, 2013

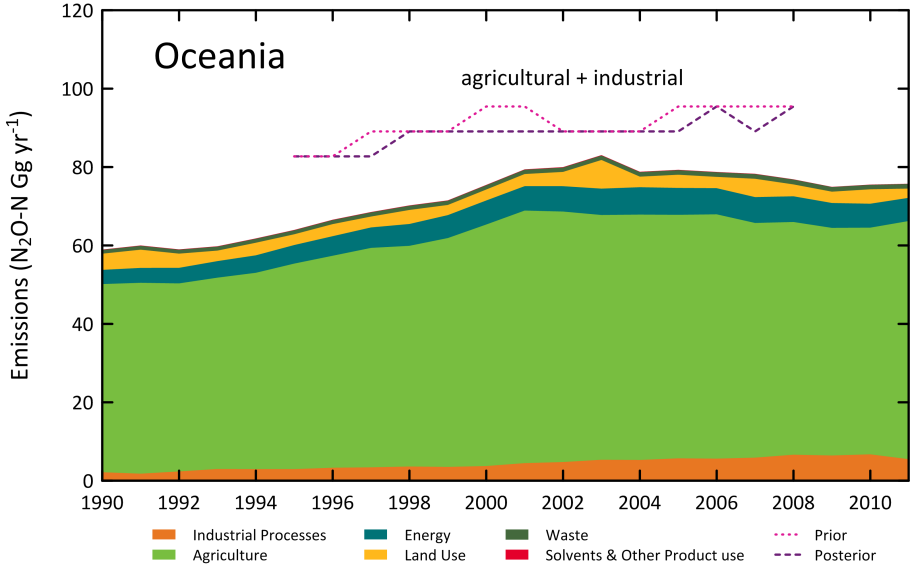

Fig. 5c. Comparison of IPCC estimates with our prior (pink dot) and optimized agricultural and industrial emissions (purple dash) in Gg N_2O–N yr^{-1} for Oceania.

ACPD
13, 19471–19525, 2013

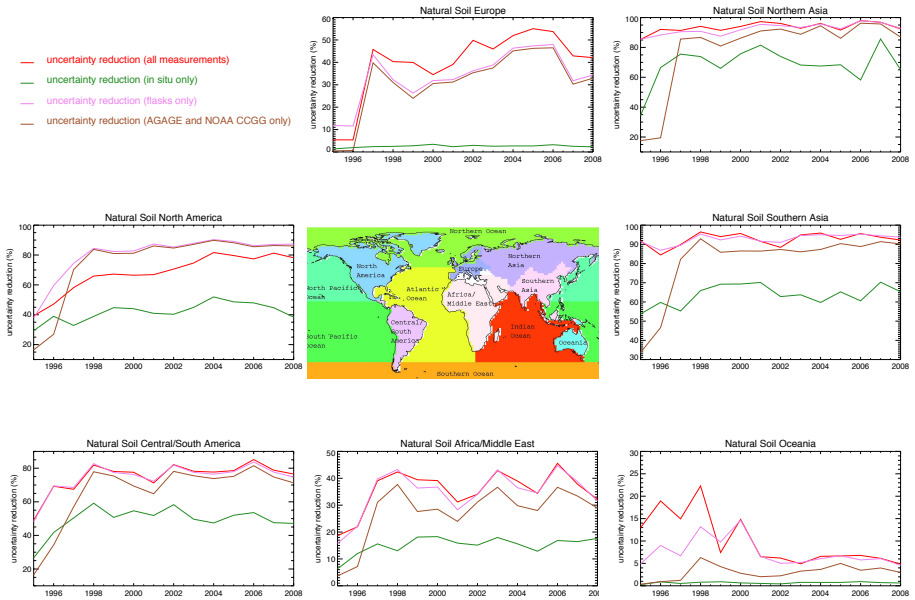

Fig. 6. Comparison of posterior natural soil emissions uncertainty reduction using different sets of measurements. The number of long-time ground measurement sites for each are as follows: all measurements (119), in situ only (12), flasks only (97), and AGAGE and NOAA CCGG only (88)

ACPD
13, 19471–19525, 2013